Final Report for a Contract Between the UNC Institute of Marine Sciences and the Albemarle-Pamlico National Estuary Partnership for work entitled:

Evaluation of water clarity metrics for protection of submerged aquatic vegetation in the Albemarle-Pamlico Estuarine System

Nathan S. Hall
University of North Carolina at Chapel Hill
Institute of Marine Sciences
Morehead City, NC
nshall@email.unc.edu
(252) 726-6841 ext. 228

16 March 2022

Version: Final

Photo credit: Rachel Gittman

Table of Contents

List of Tables

List of Figures

List of Acronyms

AICc	Akaike information criteria, corrected
AMS	Ambient Monitoring System by NCDWR
APES	Albemarle-Pamlico Estuarine System
APNEP	Albemarle-Pamlico National Estuary Partnership
Chl$a$	chlorophyll a
CHPP	Coastal Habitat Protection Plan by NCDEQ
CDOM	colored dissolved organic matter
cm	centimeter
DOC	dissolved organic carbon
ECU	East Carolina University
FNU	formazine turbidity units
K_{dPAR}	light attenuation coefficient for photosynthetically active radiation
m	meter
µg L^{-1}	micrograms per liter
ModMon	Neuse River Modeling and Monitoring Program
nm	nanometer
NAP	non-algal particulates
NCCA	National Coastal Condition Assessment by USEPA
NCDEQ	North Carolina Department of Environmental Quality
NCDMF	North Carolina Division of Marine Fisheries
NCDP	Nutrient Criteria Development Plan by NCDEQ
NCDWR	North Carolina Division of Water Resources
NE	northeast
NERRS	National Estuarine Research Reserve System
NTU	nephelometric turbidity unit
OACs	optically active constituents
PAR	photosynthetically active radiation
RMSE	root mean square error
SAC	Scientific Advisory Council for the Nutrient Criteria Development Plan
SAV	submerged aquatic vegetation
SD	Secchi disk depth
SECN	Southeast Coast Inventory and Monitoring Network
SW	southwest
UNC-IMS	University of North Carolina at Chapel Hill's Institute of Marine Sciences
USACE	U.S. Army Corps of Engineers
USEPA	U.S. Environmental Protection Agency
USGS	U.S. Geological Survey
UV	ultraviolet
YSI	Yellow Springs Instrument Inc.

1. Executive Summary

The goal of this project was to establish scientifically defensible chlorophyll *a* (Chl*a*) and turbidity thresholds that are protective of submerged aquatic vegetation (SAV) for high- and low-salinity zones of the Albemarle-Pamlico Estuarine System (APES). SAV are critical habitats that provide a host of services including nursery and feeding areas for important fisheries resources, sediment stabilization, and carbon sequestration (Harborne et al. 2006; Unsworth et al. 2010). SAV are also useful and sensitive indicators of water quality, particularly water clarity changes related to eutrophication (Dennison et al. 1993). Protection of SAV within North Carolina's estuarine waters is an important goal of the Albemarle-Pamlico National Estuary Partnership (APNEP) and the North Carolina Department of Environmental Quality (NCDEQ) including its Division of Marine Fisheries (NCDMF) and Division of Water Resources (NCDWR). Establishing Chl*a* and turbidity thresholds for SAV protection will play an important role in the process of numeric nutrient criteria development for North Carolina estuarine waters as part of the NC Nutrient Criteria Development Plan (NCDP) and will provide information for conservation and management of SAV habitats under APNEP's Comprehensive Conservation and Management Plan and NCDEQ's 2021 amendment to the NC Coastal Habitat Protection Plan (CHPP).

Availability of photosynthetically active radiation (PAR) is a primary determinant of the health and long-term survival of SAV habitats (Kemp et al. 2004). Photosynthetically active radiation declines exponentially with depth and the rate of decline is expressed as the diffuse attenuation coefficient for PAR (K_{dPAR}). K_{dPAR} is a function of PAR absorbance by phytoplankton biomass (measured as Chl*a*), but also absorption and scattering by non-algal particulate matter, absorbance by colored dissolved organic matter (CDOM) and absorbance and scattering by water itself. The primary objective of this project was to use an existing bio-optical model (Biber et al. 2008) to account for the PAR attenuation by the combination of CDOM and water, and then calculate the maximum Chl*a* concentration and turbidity thresholds that provide sufficient PAR transmission to the plants (i.e., sufficiently low K_{dPAR}) to maintain healthy low-salinity and high-salinity SAV habitats in APES. Target PAR levels for maintaining healthy SAV habitats were adopted from a compilation of SAV PAR requirements for growth (Kemp et al. 2004) and empirical observations on SAV depth distribution within APES (Biber et al. 2008; Speight 2020). These adopted clarity targets provide the transmission of 22 and 13% of incident solar radiation to depths of 1.7 and 1.5 m for high- and low-salinity SAV and correspond to K_{dPAR} values of 0.89 m^{-1} and 1.36 m^{-1}, respectively.

The bio-optical model was originally calibrated for the North River, a high-salinity estuary that has a weak hydrologic connection to the large water bodies of the APES, Pamlico and Albemarle Sounds, and their tributaries, (Giese et al. 1979). Therefore, before the model could be used across APES, this project first tested the ability of the bio-optical model to accurately predict K_{dPAR} for different high- and low-salinity waters of the APES. The bio-optical model estimates K_{dPAR} based on concentrations of three optically active water quality constituents: non-algal particulates measured as turbidity (nephelometric turbidity units or NTU), colored dissolved organic matter (CDOM) measured as absorbance at 440 nm (m^{-1}), and Chl*a* (μg L^{-1}). Validating the model's ability to accurately calculate K_{dPAR} and estimate the effect of changing Chl*a* and turbidity levels on K_{dPAR}, requires these three water quality data inputs and a corresponding dataset of directly measured K_{dPAR} values from the same water samples. Unfortunately, within the APES, there was only one dataset, other than the North River dataset used to originally calibrate the bio-optical model, that had all four parameters measured simultaneously, the Neuse River Estuary dataset collected by the Neuse River Modeling and Monitoring Program (ModMon). Turbidity and Chl*a* data were readily available for many areas throughout APES. However, direct measurements of CDOM and K_{dPAR} were scarce. To overcome the lack of CDOM and K_{dPAR} data, CDOM and K_{dPAR} data were estimated using empirical models related to salinity and water clarity measured as Secchi disk depth

(SD), respectively, and developed using available datasets from the APES including the ModMon dataset from the Neuse River and Pamlico Sound and the U.S. Environmental Protection Agency's (USEPA) National Coastal Condition Assessment (NCCA) dataset from Albemarle and Pamlico Sounds.

Secchi disk depth data are the primary data available for water clarity in the APES. Several empirical models have been developed to relate SD to K_{dPAR} but model coefficients are system specific and related to the scattering/absorbing characteristics of dissolved and particulate substances in the water, including phytoplankton (Gallegos et al. 2011). For this project, five empirical models were developed and tested to determine the most useful models for relating SD to K_{dPAR} for different regions of APES. The best models for predicting K_{dPAR} were a power function of SD that included model terms for salinity and seasonality. The models captured 78 and 72 percent of the variation of K_{dPAR} for the measurements made in the lower Neuse River and southern Pamlico Sound and the Albemarle Sound and northern Pamlico Sound, respectively and had minimal bias. Conversion of SD to K_{dPAR} by the selected models provided a large K_{dPAR} data set for assessing the performance of the Biber et al. (2008) bio-optical model for calculating the influence of Chl*a* concentration on K_{dPAR}. Additionally, it provided a large dataset for assessing the current water clarity of APES in relation to the SAV water clarity targets for high- and low-salinity SAV.

The largely freshwater source and low reactivity of CDOM in estuarine waters provides the potential for estimating CDOM based on measurements of salinity (Bowers and Brett 2008). Six empirical models were developed and tested to find models that could accurately predict CDOM for different regions of APES. The candidate models were developed using CDOM and salinity data from the ModMon dataset from the Neuse River estuary and the Biber et al. (2008) dataset from the North River estuary. For both systems, the selected models for predicting CDOM were a power function of salinity with a term that captured seasonality. The models explained 66 and 82 percent of the variance of measured CDOM in the Neuse and North River estuaries, respectively and had minimal bias across the range of measured CDOM. This indicated good predictive capability for CDOM for these estuaries. However, substantial differences in the model coefficients between the two estuaries indicated that CDOM relationships can exhibit significant cross-system variability. Thus, it is unclear how well the empirical models were capable of estimating CDOM for other regions of APES, and this remains a potentially significant source of model error and/or bias for calculated Chl*a* thresholds.

Validation of the bio-optical model was accomplished by comparing modeled K_{dPAR} with direct measurements of K_{dPAR} or estimates of K_{dPAR} derived from SD from two high-salinity estuaries, Bogue Sound and Pamlico Sound, and three low-salinity estuaries, the Neuse River, Pamlico River, and Albemarle Sound. Estimates of CDOM derived from empirical models were used as model input for waters where CDOM measurements were not available. The model moderately underestimated K_{dPAR} for the high-salinity estuaries, Bogue and Pamlico Sound, with mean bias ratios (observed: modeled K_{dPAR}) of 1.40. Underestimation of K_{dPAR} for the low-salinity estuaries, Albemarle Sound, Pamlico River, and Neuse River, was more severe with bias ratios ranging from 1.50 to 1.58. The more severe underprediction of K_{dPAR} in the low-salinity estuaries and an increasingly severe underprediction bias of K_{dPAR} along the salinity gradient from Pamlico Sound to the upper Neuse River estuary is an indication that the model is incorrectly parameterized for some aspect(s) of the absorption and/or scattering properties of optically active constituents associated with freshwater inputs to the APES. Reducing the bias will require recalibrating the bio-optical model for low-salinity waters that appear optically distinct from the North River. Resulting improvements in K_{dPAR} estimates will greatly increase confidence in the model's ability to accurately determine Chl*a* thresholds for meeting the low-salinity water clarity target. Despite the severe bias for the freshwater estuaries, there was still a tight linear relationship (just far from the 1:1 line) between observed and modeled K_{dPAR} in low-salinity waters. This tight linear relationship suggests that the model has a high likelihood of providing accurate and precise K_{dPAR} estimates once it has been properly recalibrated.

The model was used to calculate threshold levels for Chl$a$ and turbidity that will maintain K_{dPAR} at or below (note clarity decreases as K_{dPAR} increases) water clarity targets for high- and low-salinity SAV habitats described above. In the upper parts of the Neuse River, Pamlico River, Albemarle Sound and its tributaries, PAR attenuation by turbidity and CDOM was so high that water clarity targets for low-salinity SAV would not be met if Chl$a$ was reduced to zero. Chl$a$ and turbidity targets for the lower parts of the Neuse and Pamlico Rivers and eastern parts of Albemarle Sound were severely overestimated due to the model bias in low-salinity waters. Meaningful Chl$a$ and turbidity targets will be achieved for these low-salinity areas after the model is recalibrated. For high-salinity SAV habitats including Core Sound, the lower North River, Pamlico Sound, and Bogue Sound, the model indicated that threshold annual median values for Chl$a$ of 15 µg L^{-1} and turbidity of 5 NTU would generally provide sufficient water clarity.

The current numeric North Carolina water quality standards for Chl$a$ and turbidity are 40 µg L^{-1} and 25 NTU, respectively, and are currently assessed as do-not-exceed values with an allowance for 10% of samples to exceed the standard due to natural causes. A water body is considered impaired when there is 90% statistical confidence that the 90% quantile exceeds the numeric standard. A statistical analysis accounted for the observed probability distribution of Chl$a$ and turbidity in North Carolina estuaries and showed that threshold values of 15 µg L^{-1} Chl$a$ and 5 NTU turbidity would require numeric standards of 30 µg L^{-1} Chl$a$ and 10 NTU turbidity given the current assessment methodology. Thus, North Carolina's current Chl$a$ and turbidity standards, as they are being currently assessed, are not protective for North Carolina's high-salinity SAV habitats.

Median K_{dPAR} values from direct measurements, estimates based on SD, and bio-optical model outputs were compared against the water clarity targets for high- and low-salinity SAV habitats at sites throughout APES. For most of the low-salinity SAV habitats including Albemarle Sound, Currituck Sound, and the upper parts of the Neuse and Pamlico Rivers, light availability was less than 50% of the SAV light requirement. Clarity was better and low-salinity SAV light requirements were generally met in the lower parts of the Neuse and Pamlico Rivers. For high-salinity SAV habitats in Pamlico Sound, light availability was generally adequate south of Hatteras but moderately inadequate from Hatteras to Bodie Island. Core Sound and Back Sound to Beaufort Inlet generally had adequate clarity while clarity in Bogue Sound was moderately less than target levels.

Through this project, four data gaps were identified as significant impediments to further development and refinement of SAV related water clarity thresholds for APES. 1) Despite its general importance to water clarity in APES, CDOM data is largely unavailable for most areas of APES. 2) Few data exist for any of the optical indicators (turbidity, Chl$a$, CDOM) from the high-salinity SAV habitats that fringe the Outer Banks from Core Banks to Bodie Island. 3) For most of APES, few direct measurements of K_{dPAR} are available for validating the bio-optical model or developing improved, region-specific empirical models that could relate extensive SD records to K_{dPAR}. 4) Measurements of the scattering and absorption spectra, and scaling coefficients for low-salinity waters are needed to recalibrate the Biber et al. (2008) bio-optical model for development of accurate Chl$a$ and turbidity thresholds for low-salinity SAV habitats.

2. Background

SAV are critical habitats that provide a host of services including nursery and feeding areas for important fisheries resources, sediment stabilization, and carbon sequestration (Harborne et al. 2006; Unsworth et al. 2010). SAV are also useful and sensitive indicators of water quality, particularly water clarity changes related to eutrophication (Dennison et al. 1993). North Carolina's estuaries host the largest area of SAV on the U.S. East Coast, and the expansive SAV habitats play a critical role in supporting North Carolina's economically-important commercial and recreational fisheries. North Carolina's SAV habitats can be categorized functionally and by species assemblage into high- and low-salinity SAV habitats. High-salinity SAV habitats are composed of three meadow forming species, eel grass (*Zostera marina*), shoal grass (*Halodule wrightii*) and widgeon grass (*Ruppia maritima*), that occur in waters with salinity greater than 10. Low-salinity SAV habitats are composed of a larger variety of species that typically grow higher into the water column and form a canopy at the water's surface. Low-salinity SAV habitats occur at salinities less than 10, and some of the species also occur in freshwater.

Like all plants, SAV require sunlight for growth and survival. SAV light requirements are generally much higher than microalgae and macroalgae. Consequently, under nutrient rich conditions that foster rapid algal growth, algae typically outcompete SAV. SAV can handle short periods of poor light availability but chronic deficits of light availability cause SAV loss. The loss manifests as a shallowing of the maximum depth of SAV colonization and consequent reduction of SAV acreage as SAV are restricted to shallower depths under increasingly eutrophic conditions. This linkage between SAV and eutrophication makes SAV a sensitive indicator of the trophic status of estuaries (Dennison et al. 1993) and makes nutrient management of critical importance for maintaining healthy SAV habitats.

Like estuaries worldwide, North Carolina's estuaries have experienced large increases in nutrient (nitrogen and phosphorus) and sediment loading due to the activities of a rapidly growing human population in the watershed including residential development, and the expansion of agriculture, silviculture, and other industries (Mallin et al. 2000). The increased nutrient load has fueled microalgal productivity with consequent increases in concentrations of suspended phytoplankton and organic detritus in the water. The combination of high phytoplankton biomass and with elevated sediment concentrations have led to declines in water clarity that impact SAV.

In the 1980's, recurrent algal blooms within the Neuse, Tar/Pamlico, and Chowan Rivers drew attention to the issue of eutrophication within North Carolina's estuaries and nutrient load reductions were implemented in the form of a ban on phosphorus-containing detergents in the late 1980s and by improving wastewater treatment through the 1990s (Paerl et al. 2004). Since that time, an increase in non-point sources has largely erased the early gains made in nutrient load reductions (Lebo et al. 2012) and there are signs of increasing phytoplankton production in many areas of the Albemarle-Pamlico Estuarine System (APES) (NCDEQ 2021a). Since 2015, the Chowan River and western Albemarle Sound has experienced a resurgence of summer-time cyanobacteria blooms (NCDEQ 2021a). These blooms are symptomatic of a general increase in the trophic state of Albemarle Sound where Chl*a* has nearly doubled in the past 20 years and appears linked to a corresponding doubling of total nitrogen (NCDEQ 2021a). Increasing trends for Chl*a* have also been identified in the Neuse River (Van Dam and Wang 2019), though the magnitude was less severe than for Albemarle Sound.

Trends in the acreage of low- and high-salinity SAV habitats also appear to be declining. A recent hydroacoustic survey conducted throughout APES from 2014 to 2017 estimated a loss of one third of the low-salinity SAV habitat compared to the historic extent (APNEP 2020). High-salinity SAV acreage, principally along the landward side of the Outer Banks also appears to be in decline and the magnitude of decline varied significantly across regions of APES. Aerial surveys conducted in 2006-2007 and 2013

documented a 6% decline in SAV area over the seven-year period in the northern region from Roanoke Island to Hatteras Inlet, a nearly 3% decline in the central region from Hatteras Inlet to Ophelia Inlet, and an 11% decline in the southern region from Barden's Inlet to Bogue Inlet (Field et al. 2021).

These worrisome trends of eutrophication and SAV loss are made more urgent by the threats imposed by a changing climate. An increasing frequency of high intensity precipitation events is likely increasing the delivery of sediments and nutrients to APES (Paerl et al. 2019) which can cause further reductions in light availability for SAV. Additionally, warming of APES waters may have detrimental impacts on its SAV. Warmer waters lead to higher rates of respiration of organic matter within the plants and causes death if the enhanced loss of organic matter is not compensated by higher rates of photosynthesis. Consequently, the negative health impacts of decreasing light availability for photosynthesis are exacerbated as waters become warmer (Zimmerman 2006). Warming may also greatly impact the species composition and seasonal distribution of the two dominant high-salinity SAV within APES, *Zostera marina* and *Halodule wrightii*. North Carolina is a biogeographic break point for these species, being the southern limit of the temperate species *Z. marina* and northern limit of the tropical species *H. wrightii*. Summertime water temperatures in APES are already well above the temperature optima for *Z. marina* and continued warming may lead to large losses of *Z. marina* acreage as is happening currently in Chesapeake Bay (Wilson and Lotze 2019; Lefcheck et al. 2017). With the impending threats of warming, maintaining adequate water clarity for sufficient photosynthesis will be critical for maintaining SAV health throughout APES.

Protection of SAV within North Carolina's estuarine waters is an important goal of the Albemarle-Pamlico National Estuary Partnership (APNEP) and the North Carolina Department of Environmental Quality (NCDEQ) including its Division of Marine Fisheries (NCDMF) and Division of Water Resources (NCDWR). As a significant step toward improved management of SAV in APES, the APNEP SAV Team and NCDEQ's CHPP Team have collaboratively developed water clarity targets designed to ensure sufficient availability of PAR to protect both high- and low-salinity SAV. Target PAR levels for maintaining healthy SAV habitats were adopted from a compilation of SAV PAR requirements for growth of both high- and low-salinity SAV species (Kemp et al. 2004). From this compilation, targets of 22% and 13% of incident PAR were adopted for high- and low-salinity SAV habitats, respectively. To relate these PAR targets to a desirable water clarity requires establishing a target depth to which SAV growth is desired. Target depths were determined as a committee consensus of the two teams based on empirical observations of SAV depth distribution within APES. For high-salinity SAV zones, a depth target of 1.7 m was adopted based on the average deep edge depth of 1.7 m observed by Biber et al. (2008) in the North River. For low-salinity SAV zones, a target depth of 1.5 m was adopted based on observed SAV depth distributions of low-salinity waters in Albemarle Sound (Speight 2020). The combination of targets for incident PAR at 22 and 13% and SAV depth targets set at 1.7 m and 1.5 m provides the information necessary to calculate water clarity targets expressed as diffuse attenuation coefficients for downwelling PAR (K_{dPAR}) which are 0.89 and 1.36 m^{-1} for high- and low-salinity SAV zones, respectively.

To determine what management actions might be necessary to achieve these targeted levels of PAR attenuation requires knowledge of the relationships between concentrations of optically active constituents (OACs) (phytoplankton, non-algal particulates, and CDOM) and their effects on PAR attenuation in the water column. Non-algal particulates include suspended mineral sediments and organic detritus. Two different methods have been used widely to estimate the contribution of OACs to PAR attenuation. The simplest approach is to use regression analyses to empirically estimate partial attenuation coefficients for each OAC, and then assuming that the effects of each constituent are linear and the effects of the OACs together are additive, calculate the total attenuation as the sum of the constituents. This approach has been used with some success (Fernandes et al. 2018; Petus et al. 2018; Gallegos 2001) but is

error prone and can lead to biased estimates of OACs needed to achieve a targeted K_{dPAR} (Gallegos 2001). A significant problem with this approach is that the effects of the individual OACs do not vary linearly with concentration and the combined effects of the OACs are not additive (Gallegos 2001). This arises due to the non-linear interactions between absorption by all three OACs as well as pure water and scattering by non-algal particulates and phytoplankton (Kirk 1994). Additionally, covariation between OACs can create negative slopes or intercepts that have no physical meaning (Fernandes et al. 2018; Petus et al. 2018).

A second approach to decomposing the effects of OACs on PAR attenuation is to directly measure the absorption and scattering of OACs across PAR wavelengths, and then use a bio-optical model to combine the contributions of the OACs non-linearly to account for the increased pathlengths and changes in angle of light due to scattering by non-algal particulates and phytoplankton. This mechanistic modeling approach was used in this study and has been successfully used to design targets for phytoplankton biomass and non-algal particulates to protect and restore SAV in Chesapeake Bay and many other coastal waters (Biber et al. 2008; Gallegos 2001, 2005). One of these water bodies, the North River, is part of the APES. The bio-optical model was calibrated for the North River (Biber et al. 2008) based on absorption spectra of water plus CDOM, phytoplankton, and non-algal particulates, and scattering spectra of phytoplankton and non-algal particulates from North River water samples. Local calibration of the model was conducted so that the model could serve as an accurate, system-specific tool for establishing management targets for phytoplankton biomass and suspended sediments that are protective of SAV throughout the APES (Biber et al. 2008).

This project sought to answer several critical management-related questions to better understand the links between eutrophication, PAR attenuation, and SAV health across the APES.

- What threshold levels of phytoplankton biomass measured as Chl*a* and non-algal particulates measured as turbidity are compatible with maintaining sufficient light availability for high- and low-salinity SAV growth in APES?

- How do those SAV related Chl*a* and turbidity thresholds compare to the current water quality standard for North Carolina's estuarine waters, and to the current Chl*a* and turbidity concentrations observed in APES waters?

- How does current water clarity compare to clarity targets for SAV expressed as a PAR attenuation coefficient across different high- and low-salinity regions of APES?

Answers to these questions will help establish scientifically defensible Chl*a* and turbidity thresholds that are protective of SAV for high- and low-salinity zones of APES. This information is needed for the process of numeric nutrient criteria development for North Carolina estuarine waters as part of the NC Nutrient Criteria Development Plan (NCDP) and will provide information for conservation and management of SAV habitats under APNEP's Comprehensive Conservation and Management Plan and NCDEQ's 2021 amendment to the NC Coastal Habitat Protection Plan (CHPP).

3. Project Goals and Objectives

The primary goals of this project were to:

1. Use an existing bio-optical model (Biber et al. 2008) to calculate the maximum Chl*a* and turbidity thresholds that are protective of SAV water clarity targets for high- and low-salinity SAV habitats,

2. Compare Chl*a* and turbidity thresholds against the current North Carolina Chl*a* and turbidity standards for estuarine waters to evaluate whether current standards protect SAV in APES, and

3. Compare water clarity targets and thresholds for Chl*a* and turbidity against current conditions in APES to determine whether SAV light requirements are being met and how much Chl*a* and/or turbidity may need to be reduced to meet SAV needs.

Objective 1. Develop empirical models to estimate K_{dPAR}. Measurements of K_{dPAR} were needed to validate the bio-optical model used for accomplishing Goal 1, and for comparing against SAV water clarity targets to accomplish Goal 3. As with CDOM, K_{dPAR} data were available only for a few locations within APES and scarcity of these critical data necessitated development of empirical models that could estimate K_{dPAR} from the wealth of SD data that has been measured throughout APES.

Objective 2. Develop empirical models to estimate CDOM concentration. CDOM is an important contributor to PAR attenuation, particularly in low-salinity waters of APES, and is a required input to the bio-optical model needed to accomplish Goal 1. Scarcity of CDOM data necessitated the ability to estimate its concentration using empirical models based on salinity. CDOM was additionally measured directly for a small set of samples collected from Pamlico Sound.

Objective 3. Validate the bio-optical model for use in high-salinity and low-salinity waters throughout APES. The bio-optical model was originally calibrated for the North River, a high-salinity estuary that has a weak hydrologic connection to the large water bodies, Pamlico and Albemarle Sounds and their tributaries, of the APES. Therefore, before the model could be used to accomplish Goal 1, it was critical to test the model's ability to accurately predict K_{dPAR} at sites throughout the APES.

Objective 4. Use the validated bio-optical model to calculate Chl*a* and turbidity thresholds that protect water clarity for SAV habitats in APES.

Objective 5. Compare Chl*a* and turbidity thresholds derived by the bio-optical model against the North Carolina water quality standards for Chl*a* and turbidity in estuarine surface waters.

Objective 6. Compare current water clarity conditions throughout APES against water clarity targets for high- and low-salinity SAV habitats.

Objective 7. Identify data gaps that impede progress toward assessment of water clarity and establishment of SAV water clarity thresholds for waters of APES.

4. Methods

4.1. Development of an empirical relationship between SD and PAR attenuation (Objective 1)

Simultaneously measured SD and K_{dPAR} were gathered from three datasets (Table 1). The first dataset from the ModMon program consisted of more than 20 years of simultaneously collected SD and K_{dPAR} data for 11 stations along the Neuse River and nine stations in southwestern Pamlico Sound. The second dataset was the 2012-2014 U.S. Geological Survey (USGS) study (Moorman et al. 2017) within the greater Albemarle Sound region. The third dataset consisted of measurements made within the Albemarle Sound, Currituck Sound, Croatan Sound, and Pamlico Sound in 2010 and 2015 by the U.S. Environmental Protection Agency's (USEPA) National Coastal Condition Assessment (NCCA). Data from the USGS and NCCA collected in Pamlico Sound north of 35.5 °N were combined into a single dataset representing Albemarle/NE Pamlico Sound, while ModMon data and NCCA data from Pamlico Sound south of 35.5 °N were grouped into a Neuse River/SW Pamlico Sound dataset. For each of the two final datasets, empirical model development and selection were conducted on a randomly selected half of the data, while the other half was held out for validating the final selected model. The NCCA dataset also included a small set of data from the Pamlico and Pungo Rivers (N=9). This dataset was deemed too small for developing a reliable empirical model. Instead, the K_{dPAR} estimates were produced for the Pamlico and Pungo Rivers using the empirical model developed from the Neuse/SW Pamlico Sound dataset and the measured K_{dPAR} data from the Pamlico and Pungo Rivers were used to validate the empirical model derived from the Neuse/SW Pamlico Sound dataset. Similarly, unpublished SD and salinity data from Biber et al.'s (2008) study from the North River were used as input to the empirical model developed from the Neuse/SW Pamlico Sound dataset, and K_{dPAR} estimates were compared to measured K_{dPAR} to determine whether the empirical model had sufficient accuracy to be applied in other high-salinity estuarine zones.

Least squares curve fitting was used to estimate the proportionality constant κ for an inverse function, and the coefficients κ and b for a power function (Table 2); two common empirical models that relate SD to K_{dPAR} (Martin and McCutcheon 1999). The proportionality constant κ is positively related to the ratio of absorbance to scattering in a waterbody (Gallegos et al. 2011) which varies significantly along the estuarine salinity gradient of the APES (Woodruff et al. 1999). Consequently, for another set of candidate models (Table 2), κ was modeled as a linear function of freshwater fraction (F) calculated as

$$F = (S_{sw}-S)/S_{sw}$$

where S is salinity and $S_{sw} = 36$ is an assumed constant seawater salinity (Peierls et al. 2012). Seasonality of CDOM (Hounshell et al. 2019), algal blooms (Pinckney et al. 1998), and sediment resuspension (RTI 2013) may also create seasonality in κ (Gallegos et al. 2011). In another candidate model, a seasonality term was added as a sine function of the fraction of the year (fraction = 0 on 1 January and fraction = 1 on 31 December) of the sampling date (t) with a fitted amplitude (*d*) and phase (*e*) (Table 2). Models were tested that included the salinity effect, the seasonal term, and both the salinity and seasonal term together (Table 2). Akaike Information Criteria corrected for sample number (AICc) were calculated for the fits of the five different possible models shown in Table 2. Confidence intervals on model parameters were estimated by standard bootstrapping (Hall et al. 2004) with 1000 resampled data sets each of the same size as the original. The upper and lower bounds for the 95% confidence interval were then defined as the 26th and 975th rankings of each parameter estimate (Hall et al. 2004). Precision of model estimates provided additional information useful for deciding and justifying the selection of simple versus more complex models. Model residuals were also examined to determine if there were any underlying patterns in the error that might be explained by adding additional terms, or that may affect interpretation of K_{dPAR} estimates derived from the model.

Table 1. Summary of optical water quality datasets used in the study.

Purpose of Use	Program/ Study	Location	Site num.	Date range	Optical Indicators	Light measures
estCDOM estK$_{dPAR}$ avgK$_{dPAR}$ Chl$_{thresh}$	Biber et al. (2008)	North River	9	2002-2004	CDOM Turbidity Chl$a$	K$_{dPAR}$ Secchi
estCDOM estK$_{dPAR}$ Validate avgK$_{dPAR}$ Chl$_{thresh}$	ModMon	Neuse River	11	1994-pres.	CDOM Turbidity Chl$a$	K$_{dPAR}$ Secchi
estK$_{dPAR}$ Validate avgK$_{dPAR}$ Chl$_{thresh}$	ModMon	Pamlico Sound	9	1999-pres.	CDOM[1] Turbidity Chl$a$	K$_{dPAR}$ Secchi
Validate avgK$_{dPAR}$ Chl$_{thresh}$	Bogue Watch	Bogue Sound	1	2007-pres.	Turbidity Chl$a$	K$_{dPAR}$
avgK$_{dPAR}$ Chl$_{thresh}$	National Estuarine Research Reserve System	Middle Marsh Shackleford Banks	1 1	2008-pres.	Turbidity Chl$a$	Secchi
avgK$_{dPAR}$ Chl$_{thresh}$	Cape Hatteras Nat. Seashore (SE Coast Network)	Pamlico Sound at Ocracoke	1	2007-2020	Turbidity Chl$a$	Secchi
avgK$_{dPAR}$ Chl$_{thresh}$	Cape Hatteras Nat. Seashore (Wright 2016)	Sound side Outer Banks, Bodie Island to Shackleford Banks	30	July 2015	Turbidity Chl$a$	Secchi
estK$_{dPAR}$ avgK$_{dPAR}$	USGS (Moorman et al. 2017)	Albemarle/ Currituck Sounds/ tributaries	37	2012-2014	TSS[2] Chl$a$	K$_{dPAR}$ Secchi
estK$_{dPAR}$ avgK$_{dPAR}$	NCCA	NC Estuarine Waters	29 37	2010 2015	Chl$a$	K$_{dPAR}$ Secchi
avgK$_{dPAR}$	U.S. Army Corps of Engineers Duck Field Research Facility	Currituck Sound	5 2	2016-2018 2018-2019	CDOM[3] Turbidity Chl$a$[3]	K$_{dPAR}$
avgK$_{dPAR}$	NCDWR AMS	Neuse River Pamlico River Pungo River Albemarle Sound/ tributaries	9 9 3 16	1970s-pres.	Turbidity Chl$a$	Secchi
avgK$_{dPAR}$	NCDMF P120 trawl & P915 gillnet surveys	NC Estuarine Waters	417	2008-present		Secchi
avgK$_{dPAR}$	ECU Coastal Studies Institute	Albemarle/ Currituck Sounds	96	2001-2014		Secchi

For purpose of use, "estCDOM" = parameterize empirical models that estimate CDOM. "est K$_{dPAR}$ " = parameterize empirical models that estimate K$_{dPAR}$. "Validate" = validate the bio-optical model. "Chl$_{thresh}$" = determine threshold Chl$a$ concentrations for SAV protection. "avgK$_{dPAR}$ " = establish average K$_{dPAR}$ for a waterbody. [1]Measured CDOM data for Pamlico Sound consists of 45 samples as part of the current study. [2]The majority (55%) of the TSS data were left censored with a high (15-75 mg/L) method detection limit. [3]CDOM and Chl$a$ were measured as *in situ* fluorescence.

Table 2. Comparison of empirical models used to estimate K_{dPAR} from Secchi disk depth.

Model description	Model Best fit parameters (95% C.I.)	RMSE (m^{-1})	R^2_{adj}	AICc	Δ	ω
Neuse River Estuary and Southwest Pamlico Sound						
Model 1. Power function with κ as a linear function of freshwater fraction (F) and a seasonal term based on fraction of year (t)	$K_{dPAR}= (aF + c)SD^b + d\sin(2\pi(t-e))$ a = 1.62 (1.56 – 1.67) c = 0.39 (0.35 – 0.43) b = -0.60 (-0.63 – -0.57) d = 0.07 (0.06 – 0.08) e = 0.55 (0.51 – 0.58)	0.34	0.79	3422	0	1
Model 2. Power function with κ as a linear function of freshwater fraction (F). κ= aF + c	$K_{dPAR} = (aF + c)SD^b$ a = 1.58 (1.53 – 1.64) c =0.42 (0.38 – 0.46) b =-0.60 (-0.63 – -0.57)	0.34	0.78	3538	115	0
Model 3. Power function with a seasonal term based on fraction of year (t)	$K_{dPAR} = \kappa SD^b + d\sin(2\pi(t-e))$ κ = 1.64 (1.63 – 1.65) b = -0.84 (-0.87 – -0.81) d =0.06 (-0.8 – 0.07) e =0.74 (0.26 – 0.75)	0.44	0.65	6170	2748	0
Model 4. Power function	$K_{dPAR} = \kappa SD^b$ κ = 1.86 (1.84 – 1.88) b = -0.64 (-0.68 – -0.60)	0.44	0.64	6219	2797	0
Model 5. Inverse function	$K_{dPAR}= \kappa/ SD$ κ = 1.65 (1.62 –1.67)	0.46	0.62	6610	3188	0
Albemarle Sound, Currituck Sound and northern Pamlico Sound						
Model 1. Power function with κ as a linear function of freshwater fraction (F) and a seasonal term based on fraction of year (t)	$K_{dPAR}= (aF + c)SD^b + d\sin(2\pi(t-e))$ a = 0.35 (0.18 – 0.88) c = 1.34 (0.94 – 1.95) b = -0.74 (-0.82 – -0.37) d = 0.52 (-0.87– 0.74) e = 0.54 (-0.04 – 0.94)	0.70	0.72	200	0	0.98
Model 2. Power function with κ as a linear function of freshwater fraction (F). κ= aF + c	$K_{dPAR} = (aF + c)SD^b$ a = 0.47 (-0.04 – 0.99) c = 1.06 (0.69 – 1.47) b = -0.81 (-0.89 – 0.50)	0.76	0.68	208	8	0.02
Model 3. Power function with a seasonal term based on fraction of year (t)	$K_{dPAR} = \kappa SD^b + d\sin(2\pi(t-e))$ κ = 1.62 (1.43 – 2.10) b = -0.75 (-.083 – -0.37) d = 0.55 (0.32 – 0.92) e = 0.97 (-0.11 – 0.04)	0.71	0.70	212	12	0.00
Model 4. Power function	$K_{dPAR} = \kappa SD^b$ κ = 1.40 (1.26 – 1.65) b = -0.85 (-0.91 – -0.53)	0.78	0.64	223	23	0.00
Model 5. Inverse function	$K_{dPAR}= \kappa/ SD$ κ = 1.18 (1.09 – 1.32)	0.83	0.60	231	31	0.00

4.2. Development of an empirical model to estimate CDOM (Objective 2)

Most CDOM inputs to estuaries come from terrestrial forests and wetland habitats and are delivered via freshwater inputs to estuaries (Spencer et al. 2013). The organic acids that comprise CDOM are slowly degraded and CDOM exhibits a nearly conservative behavior as it is advected downstream and mixed with low CDOM-containing ocean water in estuaries. Within an estuary, the near conservative behavior can produce strong inverse relationships between salinity and CDOM concentration in estuaries that can be useful for predicting either quantity if the other is known (Bowers and Brett 2008). Data on CDOM concentrations in North Carolina estuaries are sparse, and yet CDOM is known to be an important contributor to attenuation of PAR, particularly for low-salinity waters (Vahätalo et al. 2005; Woodruff et al. 1999). Empirical relationships between CDOM and salinity were developed for the existing datasets where both were measured. These datasets included the ModMon dataset for the Neuse River and the North River (Biber et al. 2008). Empirical relationships developed from these datasets were then used to estimate CDOM concentrations for areas where salinity but not CDOM was measured (Table 3).

Table 3. Comparison of empirical models used to estimate CDOM from salinity.

Model description	Models for the Neuse River Estuary Best fit parameters (95% C.I.)	R^2_{adj}	AICc	Δ	ω
Power/ non-zero intercept for salinity with flow and season terms	$CDOM = c + aS^b + dQ + e\sin(2\pi(T-f))$ $c = 0.55\ (0.13 - 0.93)$ $a = 6.4\ (6.0 - 6.8)$ $b = 4.7\ (4.0 - 5.4)$ $d = 0.19\ (0.00 - 0.38)$ $e = 0.74\ (-0.76 - 9.2)$ $f = 0.44\ (-0.05 - 0.92)$	0.66	2344	0	0.65
Power/ non-zero intercept for salinity with season term	$CDOM = c + aS^b + e\sin(2\pi(T-f))$ $c = 0.72\ (0.36 - 1.1)$ $a = 6.4\ (6.0 - 6.8)$ $b = 4.6\ (4.0 - 5.4)$ $e = 0.79\ (0.57 - 0.97)$ $f = 0.44\ (0.38 - 0.48)$	0.66	2345	1.2	0.35
Power/ non-zero intercept for salinity with flow term	$CDOM = c + aS^b + dQ$ $c = 0.74\ (0.34 - 1.11)$ $a = 5.9\ (5.6 - 6.2)$ $b = 5.2\ (4.3 - 6.2)$ $d = 0.44\ (0.24 - 0.64)$	0.62	2404	60	0
Power/ non-zero intercept	$CDOM = c + aS^b$ $c = 1.2\ (0.9 - 1.5)$ $a = 5.8\ (5.5 - 6.1)$ $b = 5.0\ (4.2 - 5.9)$	0.61	2420	76	0
Power/ zero intercept	$CDOM = aS^b$ $a = 6.9\ (6.7 - 7.2)$ $b = 3.3\ (3.1 - 3.6)$	0.60	2430	87	0
Linear	$CDOM = c + aS$ $c = -6.2\ (-7.0 - -5.5)$ $a = 12.8\ (11.9 - 13.7)$	0.55	2509	166	0

Table 3. Comparison of empirical models used to estimate CDOM from salinity (continued).

Model description	Models for the North River Estuary Best fit parameters (95% C.I.)	R^2_{adj}	AICc	Δ	ω
Power/ non-zero intercept for salinity with flow and season terms	$CDOM = c + aS^b + dQ + e\sin(2\pi(T - f))$ $c = 0.42\ (0.03 - 0.75)$ $a = 12.2\ (7.28 - 22.7)$ $b = 1.84\ (1.26 - 2.71)$ $d = -0.012\ (-0.057 - 0.037)$ $e = 0.25\ (0.13 - 0.55)$ $f = 0.87\ (0.16 - 0.98)$	0.82	97.0	2.2	0.22
Power/ non-zero intercept for salinity with season term	$CDOM = c + aS^b + e\sin(2\pi(T - f))$ $c = 0.33\ (0.15 - 0.99)$ $a = 12.4\ (-170 - 20.1)$ $b = 1.9\ (1.3 - 35.2)$ $e = 0.26\ (0.11 - 0.64)$ $f = 0.3\ (0.22 - 0.87)$	0.82	94.8	0	0.63
Power/ non-zero intercept for salinity with flow term	$CDOM = c + aS^b + dQ$ $c = 0.32\ (0.13 - 1.2)$ $a = 12.4\ (-28.1 - 21.4)$ $b = 1.82\ (1.27 - 51.0)$ $d = -0.22\ (-0.96 - 0.16)$	0.81	99.6	4.8	0.06
Power/ non-zero intercept	$CDOM = c + aS^b$ $c = 0.25\ (0.10 - 0.41)$ $a = 12.8\ (7.5 - 26.5)$ $b = 1.9\ (1.4 - 2.7)$	0.81	98.9	4.0	0.08
Power/ zero intercept	$CDOM = aS^b$ $a = 10.7\ (5.9 - 15.4)$ $b = 1.5\ (1.1 - 1.8)$	0.79	103	8.5	0.01
Linear	$CDOM = c + aS$ $c = -0.30\ (-0.52 - -0.04)$ $a = 7.2\ (5.1 - 8.7)$	0.74	124	29	0

CDOM absorbance is not regularly monitored by the ModMon program. However, UV-vis (200-800 nm) CDOM absorbance spectra were measured as components of a Neuse River research project during a dozen sampling trips in 2007 and 2008 and on nearly all sampling trips from 2013 to 2016. In total, 640 CDOM spectra with simultaneous salinity measurements were available from 88 sampling dates across eleven stations that spanned from the freshwater head of the estuary to mesohaline conditions at the mouth where it empties to Pamlico Sound. Salinity was measured using a YSI 6600 (Yellow Springs, Inc. Yellow Springs, OH) multiparameter instrument. The absorption spectra were produced from GF/F filtered sample water on a Shimadzu UV-1700 Pharma-Spec spectrophotometer with a 0.01 m pathlength. Spectra were blank corrected using an 18 MΩ deionized water blank, and CDOM attenuation in units m^{-1} was calculated by multiplying by 2.303 and dividing by the pathlength. In keeping with the bio-optical model (Biber et al. 2008), CDOM absorption at 440 nm (CDOM a_{440}) was used as a metric of CDOM concentration.

Three empirical model formulations were initially tested for estimating CDOM from salinity: a linear regression, a power function, and a power function with a positive intercept (Table 3). Estimation of model parameters and their confidence intervals and model selection was conducted in the same manner as for the empirical models relating SD and K_{dPAR}. From these base models, additional potential explanatory variables were added. This process of developing more complicated models with greater predictive skill is described in the results.

4.3. Description of the bio-optical model (Objectives 3 & 4)

The bio-optical model (Biber et al. 2008) estimates PAR attenuation due to the absorption and scattering of water, CDOM, suspended non-algal particulates, and phytoplankton. PAR absorption by phytoplankton ($a_\Phi(\lambda)$) is related to the concentration of the pigment Chl$a$ in units μg m^{-3} through Equation 1 (Table 4) where $\Phi^*_{(675)}$ is the Chl$a$ specific absorption coefficient at a wavelength (λ) of 675 nm, and $\Phi_{(\lambda)}$ is the normalized (to the absorption at 675 nm) Chl$a$ absorption spectra across the PAR band (400 to 700 nm) characteristic of the water body. PAR absorption by CDOM (a_{CDOM}) is related to CDOM absorbance at 440 nm $a_{CDOM(440)}$ through Equation 2 (Table 4) where $-S_{CDOM}$ is the constant that describes the exponential decrease of a_{CDOM} from 400 to 700 nm. PAR absorption by non-algal particulates (a_{NAP}) is given by Equation 3 (Table 4) as a function of nephelometric turbidity units (NTU) where $a^*_{NAP(440)}$ is a constant scale factor and $-S_{NAP}$ is the constant that describes the exponential decrease of a_{NAP} from 400 to 700 nm. As shown in Equation 4 (Table 4), particulate scattering is also modeled as a function of NTU where $b_p^*_{(555)}$ is a scaling constant that relates NTU to scattering at a reference wavelength of 555 nm and η is a constant that describes the spectral shape. Total absorption is calculated as the sum of absorption by phytoplankton, non-algal particulates, CDOM, and pure water (Equation 5) and total scattering is the sum of particulate scattering and scattering by pure water (Equation 6) (Table 4). The backscattering spectrum (Equation 7, Table 4) is calculated as half the scattering by pure water plus the product of total scattering and particulate scattering scaled by the backscattering to scattering ratio (b_{bp}:b_p). The PAR attenuation spectra (Equation 8, Table 4) is calculated using an empirical model of total absorption, backscatter and the solar zenith angle (θ_o) according to Lee et al. (2005). Transmittance of incident PAR ($PAR_0(\lambda)$) to water depth (z) ($PAR_z(\lambda)$) was integrated across the 400 to 700 nm spectrum to obtain total PAR transmittance (Equation 9, Table 4), and then K_{dPAR} was calculated from PAR transmittance and depth using Beer-Lambert's law (Equation 10, Table 4). Scale factors {$\Phi^*_{(675)}$, $a^*_{NAP(440)}$, $b_p^*_{(555)}$, b_{bp}:b_p } and parameters that describe the shape of the absorption and scattering spectra { $\Phi_{(\lambda)}$, S_{CDOM}, S_{NAP}, η} for the optically active constituents were developed through the model calibration exercise conducted by Biber et al. (2008) and are provided in Table 5.

Table 4. Equations describing the bio-optical model utilized in this study.

Equation 1. $a_\Phi(\lambda) = \Phi^*_{(675)}[\text{Chl}a]\Phi_{(\lambda)}$

Equation 2. $a_{CDOM}(\lambda) = a_{CDOM(440)}\exp[-S_{CDOM}(\lambda-440)]$

Equation 3. $a_{NAP}(\lambda) = a^*_{NAP(440)}[\text{NTU}]\exp[-S_{NAP}(\lambda-440)]$

Equation 4. $b_p(\lambda) = b_p^*_{(555)}[\text{NTU}]\,[(555/\lambda)^\eta]$

Equation 5. $a_{total}(\lambda) = a_\Phi + a_{CDOM} + a_{NAP} + a_w$

Equation 6. $b_{total}(\lambda) = b_p + b_w$

Equation 7. $b_{bp}(\lambda) = b_w/2 + b_{total}\,b_p(\lambda)[\,b_{bp}{:}b_p]$

Equation 8. $K(\lambda) = [1 + 0.005\theta_o]\,a_{total} + 4.18[1 - 0.52\exp\{-10.8a_{total}\}]\,b_{bp}$

Equation 9. $PARz = \int_{400}^{700} PAR_0(\lambda)exp(K(\lambda)z)\ d\lambda$

Equation 10. $K_{dPAR} = ln(PAR_0/PAR_z)/z$

The original Biber et al. (2008) bio-optical model was coded as a spreadsheet model in Excel. While the model worked flawlessly, processing was very slow. For greater computational efficiency and ease of analysis and visualization of model outputs, the model was re-coded in MATLAB (v2017b). Outputs of the rewritten model were identical to the original Excel spreadsheet model which verified the model had been re-coded correctly (Figure 1).

Table 5. Scale factors and model parameters used in the bio-optical model from the model calibration in the North River by Biber et al. (2008).

Parameter	Description	Units	Value
$\Phi^*_{(675)}$	Chlorophyll a specific absorbance at 675 nm	$m^2\,(mg\,Chl a)^{-1}$	0.0136
S_{CDOM}	Spectral slope of CDOM	nm^{-1}	0.0144
S_{NAP}	Spectral slope of non-algal particulates	nm^{-1}	0.0093
$b_p^*_{(555)}$	Turbidity specific backscattering coefficient at 555 nm	$m^{-1}\,NTU^{-1}$	0.702
s	Ratio of backscattering to scattering	dimensionless	0.018
$a^*_{NTU(440)}$	Turbidity specific absorption coefficient at 440 nm	$m^{-1}\,NTU^{-1}$	0.0384
η	Exponent tuning spectral shape of particulate scattering	dimensionless	0.49
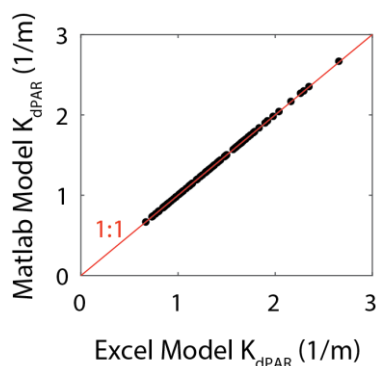
Figure 1. Demonstration of correct translation of the bio-optical model from Excel to MATLAB.

4.4. Data selection for validation of the bio-optical model (Objective 3)

Validation of the bio-optical model was accomplished by comparing modeled K_{dPAR} with direct measurements of K_{dPAR} or estimates of K_{dPAR} derived from SD from North Carolina estuarine waters. Consequently, the validation data sets required measurements or model derived estimates of the three optically active constituents used to calculate K_{dPAR} (CDOM, Chl$a$, and turbidity) as well as measured or estimated K_{dPAR} data. Other than the Biber et al. (2008) dataset from the North River where the model was originally calibrated in North Carolina, the only other water body where all four parameters were directly measured was the Neuse River Estuary as part of the ModMon program from 2007-2008 and again from 2013-2016 (Table 1). The ModMon program sampling in southwestern Pamlico Sound and the Bogue Watch monitoring program on Bogue Sound lacked CDOM measurements, so model validation was accomplished using CDOM estimates derived from empirical models (see Section 3.2). Dr. Mike Piehler's laboratory at the University of North Carolina at Chapel Hill's Institute of Marine Sciences (UNC-IMS) conducts the Bogue Watch monitoring program which is a long-term (2007 – present) approximately weekly monitoring program at one station in Bogue Sound, the UNC-IMS dock. As part of

this project, direct measures of CDOM were additionally conducted on five dates in 2020 (18 June, 14 July, 24 September, 20 October and 3 December) for the nine ModMon stations of Pamlico Sound providing a small validation dataset from Pamlico Sound with all four parameters directly measured. NCDWR Ambient Monitoring System (AMS) data collected from 2006 to 2019 were additionally used for model validation for a dataset containing four stations on the Pamlico River (stations O787000, O982500, O7650000, O8650000) and another containing six stations in Albemarle Sound (stations M390000, M610000, M7175000, D8950000, D9490000, D9995000). NCDWR's AMS conducts monthly monitoring of water quality at approximately 300 stations along NC's rivers and estuaries. For the AMS dataset, CDOM was estimated based on the empirical model related to salinity derived from the Neuse River ModMon dataset (see Section 3.2) and K_{dPAR} was estimated based on an empirical model related to SD (see Section 3.1).

Three other datasets contained direct measures of K_{dPAR} (Table 1). The USGS monitoring efforts conducted from 2012-2014 in Albemarle Sound measured K_{dPAR} and Chl$a$, but measured particulates as total suspended solids (TSS in mg/L) rather than turbidity (NTU). Relationships required for the bio-optical model between turbidity (NTU) and TSS (mg/L) were explored for samples collected in the greater Albemarle Sound region using NCDWR's AMS data set (Figure 2). The relationships were modestly strong for stations in Albemarle Sound (R^2 = 0.41-0.46) and Alligator River (R^2 = 0.44) but were poor for western Albemarle Sound (station D9995000, R^2 = 0.21) and two Chowan River stations with R^2 = 0.06 and R^2 = 0.11 (Figure 2). None of these relationships are strong enough for confident prediction of turbidity based on the USGS's TSS measurements (Prairie 1996). Additionally, most (55%) of the TSS data collected during the USGS study were determined as below the method detection limit which ranged from 15- 75 mg/L. Given the weak relationship between TSS and turbidity, and the uncertainty that the censored TSS data would introduce to any estimate of turbidity derived from TSS, the USGS dataset was rejected for validating the bio-optical model.
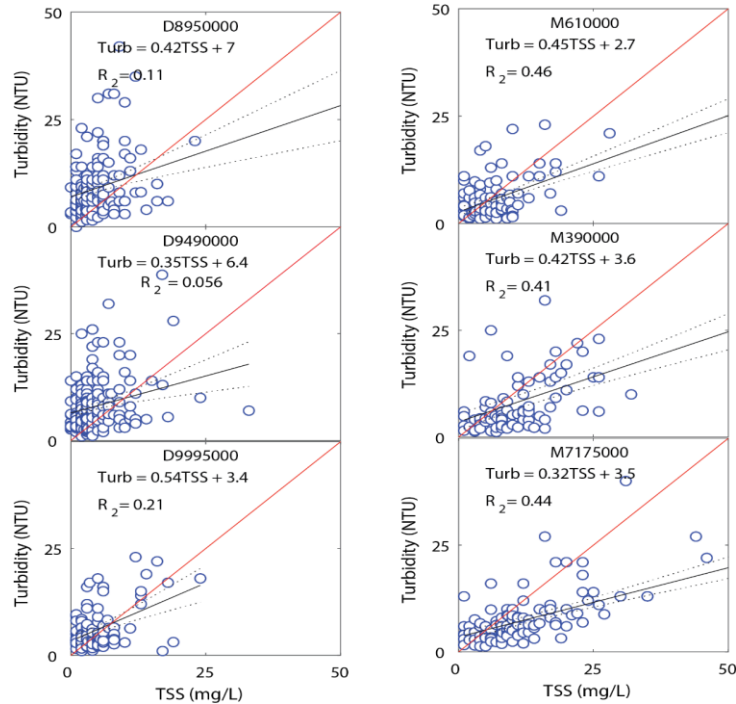
Figure 2. Linear regressions of turbidity on total suspended solids from the Chowan River (stations D895000, D949000), Albemarle Sound (D9995000, M610000, M390000) and Alligator River (M7175000) from data collected by NCDWR's Ambient Monitoring System from 1997-2019.

The U.S. Army Corps of Engineers (USACE) datasets from Currituck Sound were also rejected for validating the bio-optical model because the Chl$a$ and CDOM data were in raw fluorescence units and would require post-calibration to units of Chl$a$ (μg/L) and CDOM (a_{440}) for use in this project. Monitoring data provided by the NCCA included Chl$a$ and K_{dPAR} but could not be used for validation due to not having measurements of either turbidity or CDOM.

4.5. Establishing Chl$a$ and turbidity thresholds for high- and low-salinity SAV zones (Objective 4)

In a forward prediction mode, the bio-optical model takes inputs of the three optical water quality indicators (Chl$a$, turbidity, and CDOM) and outputs an estimate of K_{dPAR}. However, if a target value for K_{dPAR} is known, and the concentrations of two of the optical indicators can be established, a powerful utility of the model is the ability to invert the model to determine the quantity of the unknown indicator that will achieve the K_{dPAR} target. For several high-salinity and low-salinity estuarine SAV habitats, the bio-optical model was inverted to calculate Chl$a$ and turbidity thresholds that correspond to the highest possible Chl$a$ or turbidity concentration that still meets the water clarity target of 22% of incident PAR transmittance to a depth of 1.7 m ($K_{dPAR} = 0.89$ m^{-1}) for high-salinity zones and 13% of incident PAR transmittance to a depth of 1.5 m ($K_{dPAR} = 1.36$ m^{-1}) for low-salinity zones. Background attenuation due to CDOM and turbidity for calculating Chl$a$ thresholds or CDOM and Chl$a$ for calculating turbidity thresholds were input to the model as median values. Thus, Chl$a$, turbidity, and CDOM data were required for estimating both Chl$a$ and turbidity thresholds. Except for the North River and the small amount of data collected from Pamlico Sound as part of this study, CDOM was estimated based on empirical relationships with salinity.

The bio-optical model was inverted by finding the Chl*a* or turbidity value that minimized the absolute difference between modeled K_{dPAR} and the water clarity target of 0.89 m^{-1} using the bounded minimization (*'fminbnd'*) function in MATLAB. The lower bound for the Chl*a* or turbidity thresholds were set at 0 to prevent meaningless negative solutions and the upper bound was set at 1000 so that it would be irrelevant. In addition to concentrations of optically active constituents, PAR attenuation also depends on the solar zenith angle. For calculating Chl*a* and turbidity thresholds, the solar zenith angle was chosen to represent noon time sun at the spring equinox. This angle was chosen as a moderate zenith angle between the low angle of winter sun and near vertical angles of summer and provides a reasonable approximation of the solar zenith angle for a year-round SAV growing season resulting from the co-occurrence of temperate and tropical SAV species in North Carolina (Gallegos, C. pers. comm.).

Nine data sets representing different high-salinity estuarine locations were assessed (see map in Figure 15 in results section). Two of the nine datasets were comprised of data from the lower (stations 1-5) and upper (stations 6-9) North River Estuary during the Biber et al. (2008) study which were treated separately due to the near absence of SAV in the upper estuary. The Bogue Watch program (directed by Dr. Michael Piehler) monitored a Bogue Sound station (UNC-IMS pier) approximately weekly for turbidity and salinity. Middle Marsh and Shackleford Banks near Beaufort Inlet and Pamlico Sound north of Ocracoke Village were monitored through cooperative partnerships with the Cape Hatteras/Cape Lookout National Seashore and the National Estuarine Research Reserve System (NERRS) as part of the National Park Service's Southeast Coast Inventory and Monitoring Network (SECN). Turbidity and salinity at these three sites were autonomously monitored every 15 minutes using either a YSI6600 or newer Xylem EXO multiparameter water quality instruments and Chl*a* was measured approximately monthly. Data were marked with quality control codes according to SECN protocols. Data coded as "unusable", "poor quality", or "undefined" were removed from the datasets. The YSI 6600 instruments reported turbidity data as NTU while the Xylem EXO reported turbidity in formazine nephelometric units (FNU). Because both instruments used an identical technology (YSI Technical Instructions 2019) compliant with the European turbidity standard (ISO7027) and were calibrated using identical formazine standard, the FNU and NTU units were assumed equivalent and reported as NTU. Turbidity data were smoothed by calculating a daily arithmetic mean. CDOM was estimated for these stations using instantaneous salinity values as input to empirical models, and the estimated CDOM values were subsequently smoothed by taking a daily mean. For turbidity and CDOM, median values of the daily means were used as measures of average conditions to calculate Chl*a* thresholds using the bio-optical model.

Cape Hatteras/Cape Lookout National Seashore staff conducted a synoptic sampling event as part of the SECN in July 2015 that covered 30 sites from Bodie Island in the northeast of Pamlico Sound to Beaufort Inlet in the southwest (Wright 2016). Sites north and east of Cedar Island, sites 1-18 in Wright (2016), were grouped to represent Pamlico Sound on the sound side of the Outer Banks (see map in Figure 15 in the results section). For these sites and the other Pamlico Sound sites described below, CDOM was estimated based on the empirical model developed from the Neuse River. Sites 19-30 in Wright (2016) were grouped to represent Core and Back Sounds along the sound side of Core and Shackleford Banks (see map in Figure 15). For these sites, CDOM was estimated based on the empirical model developed from the North River. ModMon's Pamlico Sound dataset represented the southwest portion of Pamlico Sound from the mouth of the Neuse River to Ocracoke Inlet.

Chl*a* and turbidity thresholds for eight low-salinity estuarine zones were estimated by the bio-optical model using a combination of data collected by AMS and ModMon. Western Albemarle Sound was represented by AMS stations D9995000 and N9700000 while eastern Albemarle Sound was represented by stations M610000 and M390000. The Chowan River was represented by stations D8356200, D895000 and D949000. Other tributaries to Albemarle Sound were grouped and included Alligator River

(M7175000), Pasquotank River (M2750000), Perquimans River (M500000), Scuppernong River (M6980000) and Little River (M350000). The Neuse River was divided into two sections: the upper river comprised by ModMon stations 0, 20, 30, 50, 60 and 70, the lower Neuse River represented by stations 100, 120, 140 160 and 180. The upper Pamlico River was represented by AMS stations O765000, O7680000, O7710000, and O787000 and the lower Pamlico River was represented by AMS stations O8498000, O8650000, O9059000, and O982500. Only data collected within the past 20 years were used for estimating Chl*a* and turbidity thresholds for either low-salinity or high-salinity SAV areas.

A main source of uncertainty for Chl*a* thresholds was the error associated with median values of turbidity, and CDOM which can be substantial, particularly for small datasets such as those for high-salinity waters. For both high- and low-salinity areas, bootstrapping was used to characterize the uncertainty in Chl*a* thresholds associated with estimating the average background levels of turbidity and CDOM. Chl*a* thresholds were estimated 1000 times based on median values of resampled turbidity and CDOM datasets with replacement. The 95 percent confidence interval was then determined as the 26th and 975th ranks of the calculated Chl*a* threshold values (Hall et al. 2004). The same procedure was used to estimate uncertainty of turbidity thresholds based on error associated with median values of Chl*a* and CDOM.

4.6. Comparing Chl*a* and turbidity thresholds from the bio-optical model to the current North Carolina standard for Chl*a* and turbidity in estuarine waters (Objective 5)

The Chl*a* thresholds calculated by the bio-optical model should be interpreted as median values since they were calculated based on median turbidity and CDOM levels. Similarly, turbidity thresholds were calculated based on median Chl*a* and CDOM. The current state standard for Chl*a* in estuarine waters is 40 μg L^{-1} and for turbidity is 25 NTU. For both parameters, an allowance is made for the natural occurrence of a small, 10% frequency of exceedances. Another way of stating this standard is that the 90% quantile of the Chl*a* and turbidity distribution for a water body cannot exceed 40 μg L^{-1} and 25 NTU, respectively. Additionally, the current assessment approach requires 90% confidence that the 90% quantile exceeds 40 exceed 40 μg L^{-1} or 25 NTU before a water body is determined to be impaired and placed on the USEPA 303d list of impaired waters (NCDEQ 2021b). This creates a problem for assessing whether the current standard is sufficiently protective to meet the newly derived thresholds for SAV habitats because the thresholds and current standards are expressed for different quantiles of the Chl*a* and turbidity distributions.

The number of exceedances required to achieve a 90% statistical confidence changes based on the number of measurements made within each water body during an assessment period. For example, with a sample size of 100, 14 samples that exceed the standard would achieve a 90% statistical confidence but a sample size of 20 would require 4 exceedances, or a critical quantile of 20%, to achieve 90% confidence that the water body was impaired. Assessments of North Carolina surface water data for 303d listing are conducted on available data over a period of two years with the last year ending two years prior to the date of the assessment. For example, the 2022 assessment will be based on data collected during 2019 and 2020. Given the predominance of a monthly sampling interval for water quality monitoring, for many estuarine sites only about 24 samples are expected to be collected during an assessment period (Figure 3), and the critical quantile (i.e., value which would be considered impaired considering the uncertainty related to sample size) required for listing a water body as impaired is significantly higher than 10%.
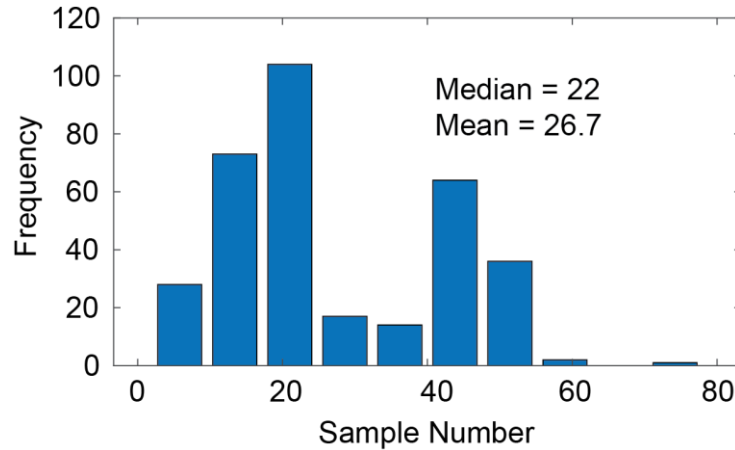
Figure 3. Histogram of sample number for Chl*a* and turbidity measurements for monitoring stations in North Carolina estuarine waters during 2-year assessment periods for determining whether a water body is impaired and should be added to the USEPA 303(d) list.

An empirical approach was taken to understand the relationship between the median Chl*a* and turbidity versus Chl*a* and turbidity values at the critical quantiles for sites throughout North Carolina estuarine waters. Chl*a* and turbidity data sets used for these analyses included data from 52 stations within the following datasets: 1) NCDWR's AMS at 9 stations spanning the Albemarle Sound and its tributaries, and the Pamlico River (D8950000, D9490000, D9995000C, M610000C, M390000C, M7175000, O787000, O8650000, O982500), 2) 11 stations from the ModMon dataset for the Neuse River and 9 ModMon stations in Pamlico Sound, 3) the high-salinity datasets used to establish the Chl*a* threshold less the synoptic survey of eastern Pamlico Sound from Wright et al. (2016), and 4) a 10-year (2007-2016) dataset from 8 stations in the New River Estuary collected as part of the Defense Coastal/Estuarine Research Program (description in Hall et al. 2013). Data from each of the 52 sites were divided into nine, two-year non-overlapping assessment periods: 2001-2002, 2003-2004, 2005-2006, 2007-2008, 2009-2010, 2011-2012, 2013-2014, 2015-2016, and 2017-2018. Treating each site and assessment period as a separate unique dataset resulted in a total of 345 datasets for the following analyses.

For each dataset, the median value of Chl*a* (or turbidity) was plotted against the Chl*a* (or turbidity) value at both the 90% quantile and the critical quantile given the sample size. Comparison against the 90% quantile simulates the best-case scenario that occurs with very high sample numbers and negligible statistical uncertainty. Critical quantiles were determined in the same manner as used by NCDEQ (2021b) by calculating the minimum exceedance percentage with a cumulative probability greater than 0.9 for a given sample size using the binomial cumulative distribution function. Comparison against the critical quantiles represents the real-world scenario where small sample sizes can significantly reduce statistical confidence with an exceedance percent much higher than 10% required to declare a waterbody as impaired. A linear regression model was used to estimate the Chl*a* and turbidity values at the 90th quantile and critical quantiles that correspond to Chl*a* and turbidity thresholds calculated using the bio-optical model. Using the regression to translate the median thresholds defined by the bio-optical model into the 90th and critical quantiles for assessment of impairment provides a useful comparison to determine whether the current standards for Chl*a* and turbidity are protective of SAV light requirements.

4.7. Comparing current water clarity with SAV water clarity targets throughout North Carolina estuarine waters (Objective 6)

Best available estimates of K_{dPAR} were used to compare current water-clarity conditions to the water-clarity thresholds for high- and low-salinity SAV zones throughout North Carolina estuarine waters. Direct K_{dPAR} values were used for sites where direct measurements were routinely made. For low-salinity sites, estimates of K_{dPAR} derived from empirical models based on SD were used. For high-salinity waters, where SD often exceeded water depth and the bio-optical model more accurately predicted K_{dPAR}, K_{dPAR} was calculated using the bio-optical model. The central tendency of recent water-clarity conditions was calculated as the median percent of incident PAR transmitted to 1.5 m and 1.7 m within low- and high-salinity SAV zones, respectively. For each station, the median percent PAR transmittance was expressed as the fraction of the low- and high-salinity SAV requirement, 13% and 22% incident light, so that values greater than 1 indicate clarity that meets the thresholds, and values less than 1 indicate clarity insufficient to permit SAV colonization to the target depths.

The dividing lines for delineating low-salinity zones in the tributary estuaries were established through consensus between the APNEP SAV Team and the NCDEQ CHPP Team charged with development of an SAV issue paper for the 2021 CHPP amendment. Low-salinity zones were defined based on absence of high-salinity SAV species and had average salinity less than 10. The dividing line between the low-salinity Neuse River Estuary and high-salinity Pamlico Sound was drawn from Point of Marsh on the south side (35.075°N, -76.470°W) to Maw Point on the north side (35.1508°N, -76.537°W), and the dividing line between Bay River and Pamlico Sound extended from Maw Point northward to Bay Point (35.185°N, -76.527°W). The dividing line between the low-salinity waters of Pamlico River and Pamlico Sound extended from Pamlico Point on the south (35.185°N, -76.527°W) to a point south of Spencer Bay (35.372°N, -76.471°W) on the north side. Croatan Sound was considered low salinity with a dividing line at the southern end of Roanoke Island at 35.824°N latitude. Roanoke Sound north and south of the highway U.S. 264 bridge was considered low and high salinity, respectively.

5. Results and Discussion

5.1. Empirical models of PAR attenuation based on Secchi disk depth (Objective 1)

For both the Neuse/SW Pamlico Sound and Albemarle/NE Pamlico Sound datasets, all five candidate models explained more than 60% of the variability in K_{dPAR} from SD (Figures 4 and 5, Table 2). The power function model (Model 4, Table 2) with an exponent of -0.64 for the Neuse River/SW Pamlico Sound and -0.85 for Albemarle/NE Pamlico Sound datasets provided modest improvements compared to the simpler inverse model (Model 5, Table 2). Examination of the residuals showed the improved fit largely resulted from correcting the inverse function's underprediction of K_{dPAR} at the deepest SD (Figure 5). Compared to the inverse model (model 5), modeling κ as a linear function of freshwater fraction (Model 2) increased the model R^2_{adj} from 0.60 and 0.62 to 0.68 and 0.78, respectively, for the Albemarle/NE Pamlico Sound and Neuse/SW Pamlico Sound datasets (Table 2).
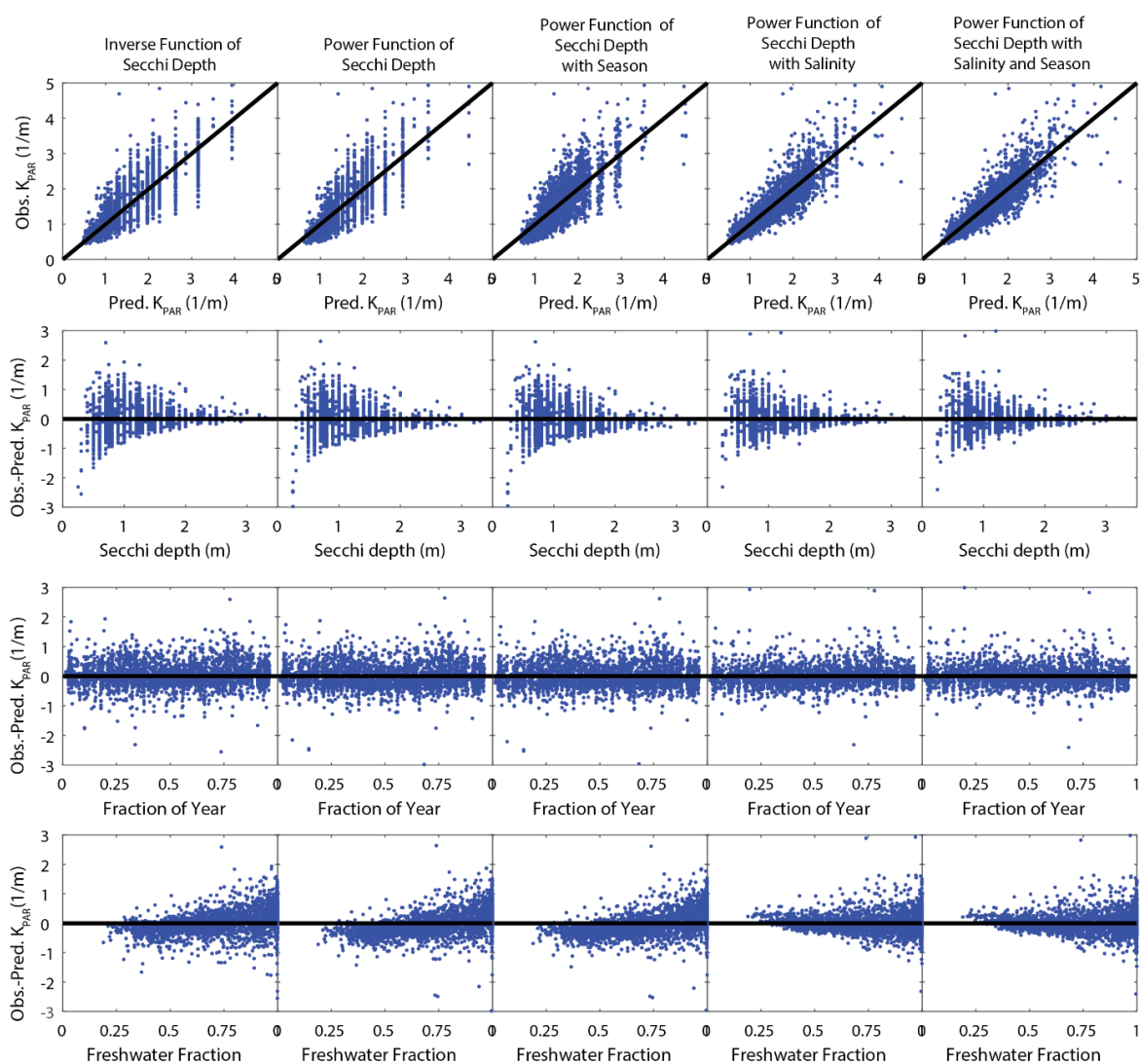
Figure 4. Comparison of empirical models and examination of residuals for empirical models used to estimate K_{dPAR} from SD for the waters of the Neuse River and southwest Pamlico Sound.
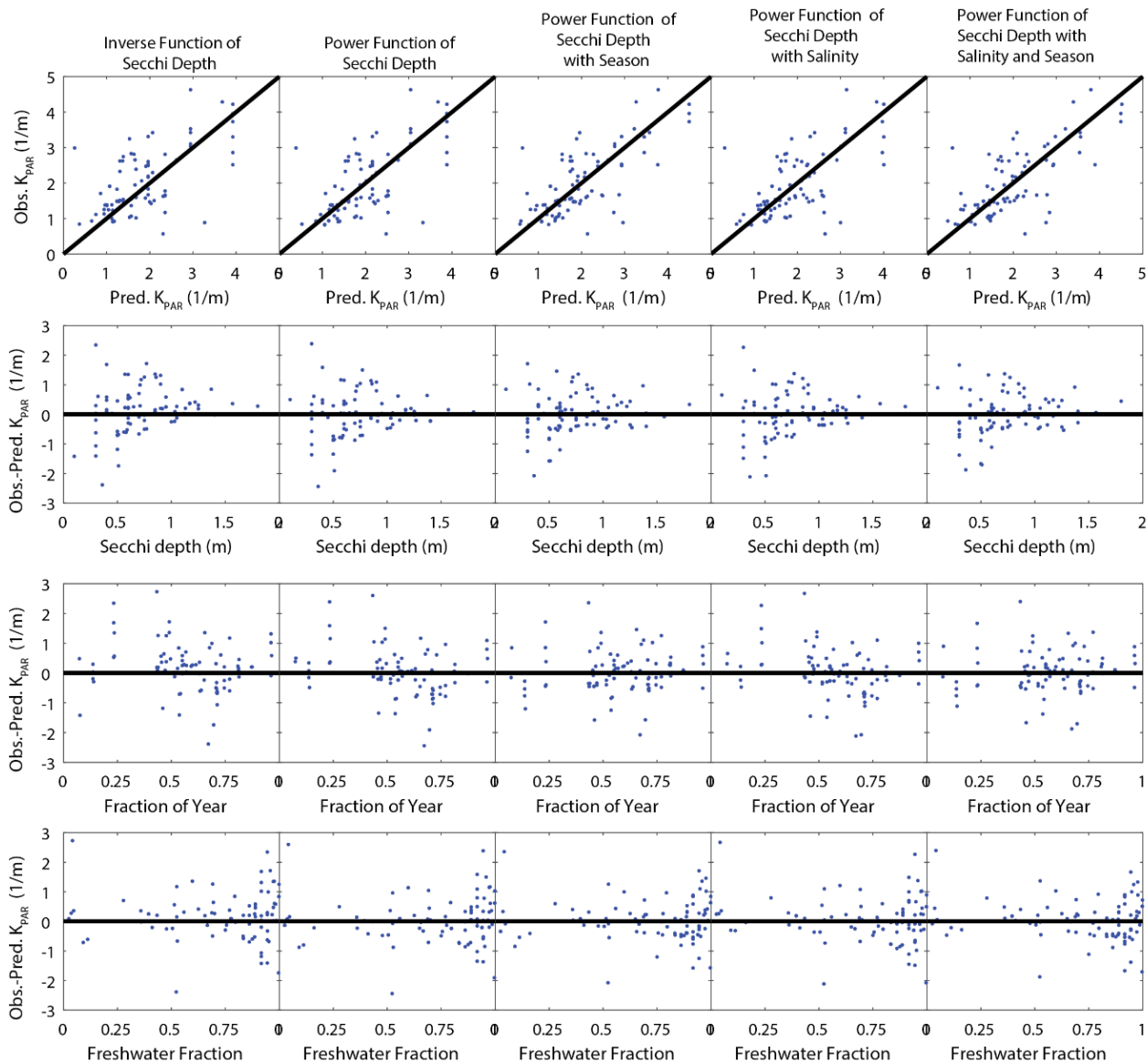
Figure 5. Comparison of empirical models and examination of residuals for empirical models used to estimate K_{dPAR} from SD for the waters of Albemarle Sound, Currituck Sound, and northern Pamlico Sound.

For the Neuse/SW Pamlico Sound dataset, residuals plotted against salinity as freshwater fraction clearly showed that the models that did not include salinity significantly overestimated K_{dPAR} at lower freshwater fraction (higher salinity) and underestimated K_{dPAR} at higher freshwater fraction (lower salinity). Addition of a seasonal term to the model that included salinity (Model 1, Table 2) provided some additional improvement in model predictions. AICc scores showed that the power function models that accounted for both salinity and seasonality were superior to models that included only one of these parameters. The models that included season but did not include the salinity effect (Model 3, Table 2), only slightly outperformed the power function model without either salinity or seasonal effects (Model 2, Table 2).

27

For the Neuse/SW Pamlico Sound dataset, the coefficient estimates for the empirical model that contained both salinity and seasonal effects (Model 1) showed a high degree of precision with 95 % confidence intervals that generally spanned < 10% of the values (Table 2). The coefficients for this model were also similar to the coefficients for the simpler models that were combined to produce it, another indication of model robustness (Models 2-5, Table 2). Model coefficients for the Albemarle/NE Pamlico Sound dataset were less precise than for the Neuse/SW Pamlico Sound dataset, likely a result of smaller sample size and poorer overall model fit (Table 2, Figure 5). Nevertheless, the model coefficients between the Neuse/SW Pamlico Sound and Albemarle/NE Pamlico Sound derived models that contained both season and salinity (Model 1, Table 2) generally agree well and indicate similar drivers of the relationship between K_{dPAR} and SD across the two estuarine regions. Due to their superior performance, the models that included both the salinity and seasonal effects (Model 1, Table 2) were selected for estimating K_{dPAR} from SD. The model developed from the Albemarle/NE Pamlico Sound data were used in conjunction with AMS SD data to estimate the recent average K_{dPAR} for stations in the Albemarle Sound region, and the model developed from the Neuse/SW Pamlico Sound dataset, that was validated using the small dataset from the Pamlico/Pungo Rivers, was used to estimate K_{dPAR} for stations on the Pamlico River.

The tendency for a higher K_{dPAR} for a given SD in low-salinity samples was captured within both the Neuse/SW Pamlico Sound and Albemarle/NE Pamlico Sound derived model by the highly significant slopes (1.58 and 0.35, respectively) for freshwater fraction (a) in the linear function used to describe κ (Table 2, Models 1 and 2). κ is positively related to the ratio of absorption to scattering of PAR and is a useful indicator to determine whether relationships between SD and K_{dPAR} are similar between water bodies (Gallegos et al. 2011). The finding that κ was higher for the low-salinity samples is consistent with previous findings that the relative importance of PAR absorption increases as absorption by CDOM and Chl*a* increase upstream along the Neuse River/Pamlico Sound estuarine gradient (Woodruff et al. 1999). At low salinities, models for both regions approach κ values near 2 but the Neuse/SW Pamlico Sound model achieves this with a higher slope (*a*) and lower intercept (*c*) than the model for the Albemarle/NE Pamlico Sound dataset. The seasonal term within the best-fit models predicts elevated K_{dPAR} during late summer and was stronger for the Albemarle/NE Pamlico Sound dataset than for the Neuse/SW Pamlico Sound dataset. This seasonality likely reflects the timing of the annual maximum of CDOM concentrations in freshwater inputs to the Neuse River/Pamlico Sound system (Hounshell et al. 2019, and Section 3.2).

Differences in the scattering-to-absorption ratio within the low-salinity samples could also explain the higher degree of model error in the low-salinity samples that had shallow SD. At the head of the Neuse River Estuary and Albemarle Sound, the Neuse River and Roanoke Rivers are hybrids of piedmont brown water rivers with moderate suspended sediment concentrations, and coastal plain blackwater rivers with high CDOM concentrations. The upper parts of these estuaries also commonly experience phytoplankton blooms (Peierls et al. 2012). The optical characteristics of the upper estuarine regions are dependent on hydrological conditions that modulate blooms through nutrient loading but also flushing (Peierls et al. 2012). The amount of flow and the relative proportions of flow coming from highly scattering, sediment-rich but CDOM-poor piedmont waters versus strongly absorbing CDOM-rich but sediment-poor coastal plain waters also play a large role in the relative importance of absorption versus scattering in North Carolina estuaries (Vahätalo et al. 2005). Thus, a wide range of backscattering-to-absorption characteristics occur in the low-salinity waters, and it should be expected that relationships between K_{dPAR} and SD might be weaker in the low-salinity waters.

The best-fit power function models that included a linear dependence on salinity and a seasonal term were validated against the hold-out datasets (see Section 2.1 for details). For the Neuse/SW Pamlico Sound model, model fit to the validation dataset was nearly identical to the calibration

dataset with the model predictions explaining 79% of observed variation in K_{dPAR} and even having a slightly lower (0.32 vs 0.34 m^{-1}) root mean squared error (Figure 6, Table 2). Mean absolute error near zero (0.004 m^{-1}) and a mean bias ratio (predicted/observed K_{dPAR}) near one indicated that the model bias was negligible (Figure 6). For the Albemarle/NE Pamlico Sound model, the fit of the validation model was significantly weaker than the fit for calibration with an increase in root mean squared error (RMSE) from 0.70 to 0.77 m^{-1} and a decrease in the adjusted R^2 from 0.7 to 0.38 (Figure 6). A decrease in fit between calibration and validation is expected and the more severe decrease with the smaller Albemarle/NE Pamlico Sound dataset is also expected because with smaller datasets a few outlier values can exert more significant influence on estimation of the model parameters. Despite the poorer model fit, plots of observed versus predicted K_{dPAR} fall along the 1:1 line throughout the range of K_{dPAR} values (Figure 6). Also, the mean absolute error was low (0.08 m^{-1}) and the bias ratio was near one (1.11) (Figure 6).
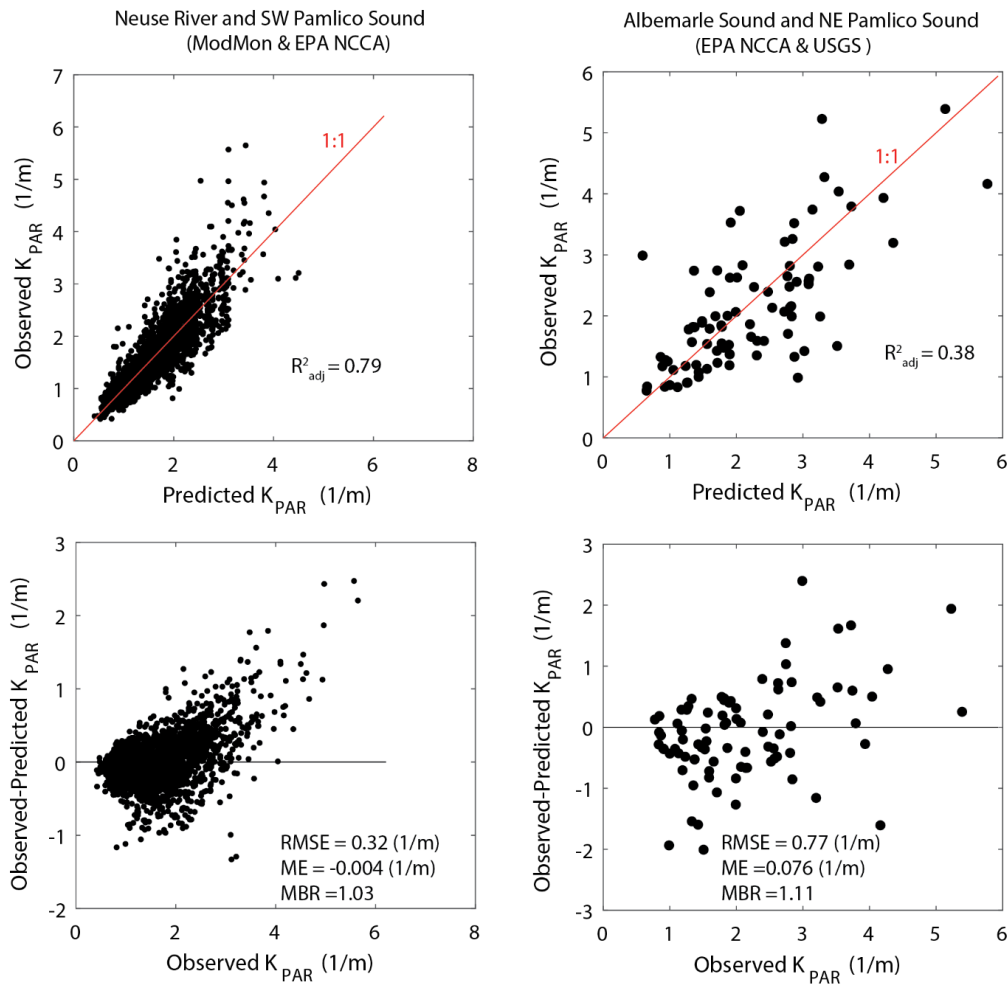
Figure 6. Validation of an empirical model developed to estimate K_{dPAR} based on SD, salinity, and time of year for datasets from ModMon and NCCA in the Neuse River and southwestern Pamlico Sound (left panels) and from the NCCA and USGS in Albemarle Sound and northeastern Pamlico Sound (right panels). Bottom panels show residuals versus observed K_{dPAR} and provide root mean squared error (RMSE), mean error calculated as predicted minus observed values (ME), and mean bias ratio (MBR) calculated as predicted divided by observed values.

Estimates of K_{dPAR} for the Pamlico River and Pungo River predicted using the model developed from the Neuse River/SW Pamlico Sound dataset were also reasonably accurate and precise. Observed and predicted values clustered near the 1:1 reference line, error was moderate with a RMSE of 0.53 m^{-1}, and with a mean absolute error (-0.04 m^{-1}) near zero (-0.04 m^{-1}) and low mean bias ratio (1.04), there was no indication of significant bias (Figure 7). The ability of the empirical model developed from Neuse/SW Pamlico Sound to reasonably predict Pamlico and Pungo River K_{dPAR} is consistent with similar patterns of scattering versus absorption along the salinity gradient of these estuaries (Woodruff et al. 1999). Surprisingly, the model developed from the Neuse River/SW Pamlico Sound dataset also reasonably predicted K_{dPAR} from SD for the North River (Biber et al. 2008) dataset though with a slight, 7% on average, underprediction as shown by the mean bias ratio (Figure 7).
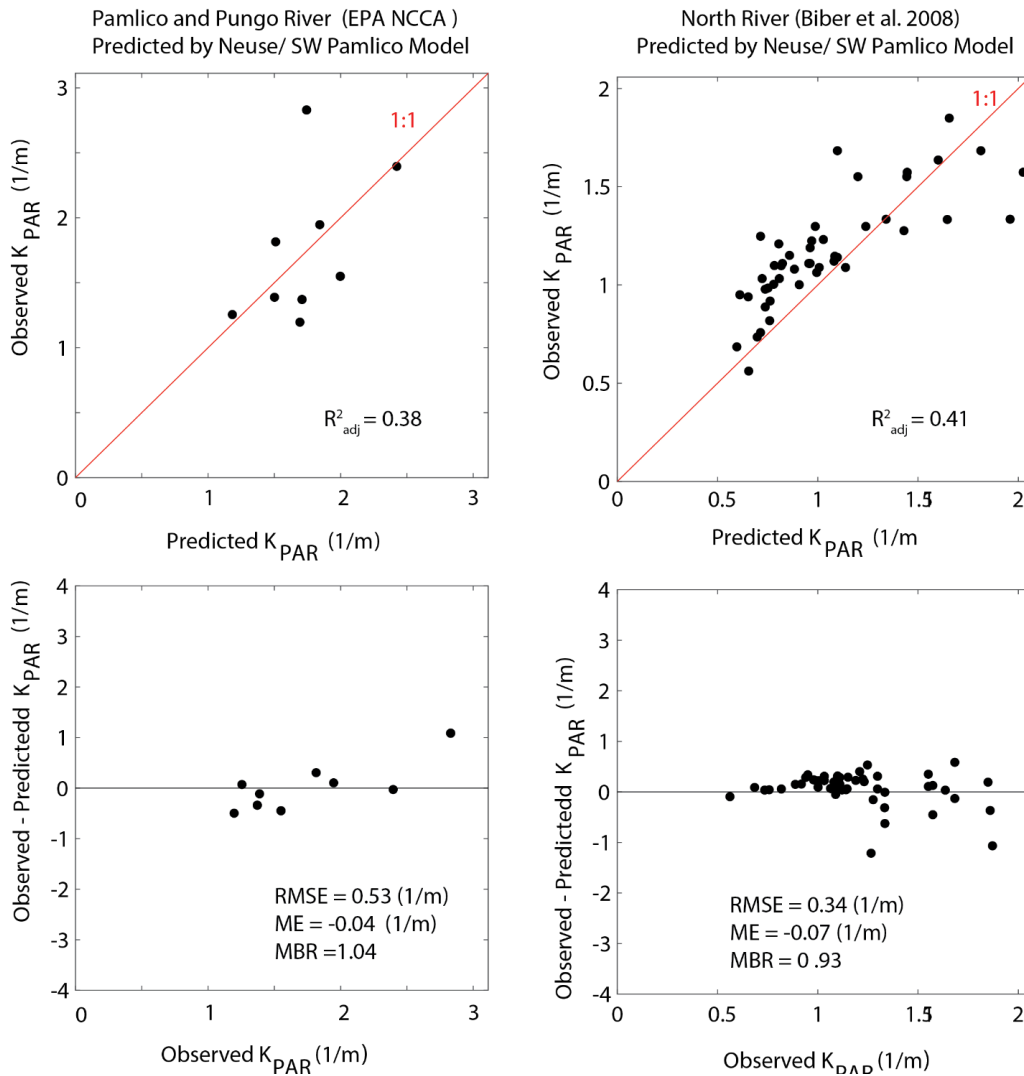
Figure 7. Test of the ability of the empirical model developed from the Neuse/southwest Pamlico Sound to predict K_{dPAR} based on SD, salinity, and time of year for the Pamlico and Pungo Rivers (left panels) and the North River (right panels). Bottom panels show residuals versus observed K_{dPAR} and provide root mean squared error (RMSE), mean error calculated as predicted minus observed values (ME), and mean bias ratio (MBR) calculated as predicted divided by observed values.

Collectively, the comparisons of measured vs estimated K_{dPAR} indicate that the empirical models based on SD and salinity produce reasonably accurate, though not especially precise K_{dPAR} estimates. Given their low degree of bias, the estimates should be suitable for validating the bio-optical model and for establishing the long-term average light conditions for SAV habitats where K_{dPAR} measurements are scarce or non-existent.

5.2. Empirical models of CDOM based on salinity (Objective 2)

The linear regression model of CDOM on salinity explained 55% and 74 % of the variability in CDOM for the Neuse River and North River estuaries, respectively (Table 3). For both estuaries, however, the linear model consistently underestimated CDOM at high salinities (low freshwater fraction), and overestimated CDOM at low salinities (high freshwater fraction) (Figure 8). At the highest salinities, the linear model predicted negative CDOM values for both estuaries. A model that predicts negative CDOM values would not be useful for deriving CDOM input to the bio-optical model. Alternatively, the zero-intercept power function model asymptotes to zero and therefore cannot predict negative CDOM values. For both estuaries, this model performed better than the linear model, explaining 60% and 79 % of CDOM variation for the Neuse and North Rivers, respectively (Table 3). Although it gave much better estimates of CDOM at high salinity than the linear model, it tended to produce slight underestimates at high salinities (Figure 8).
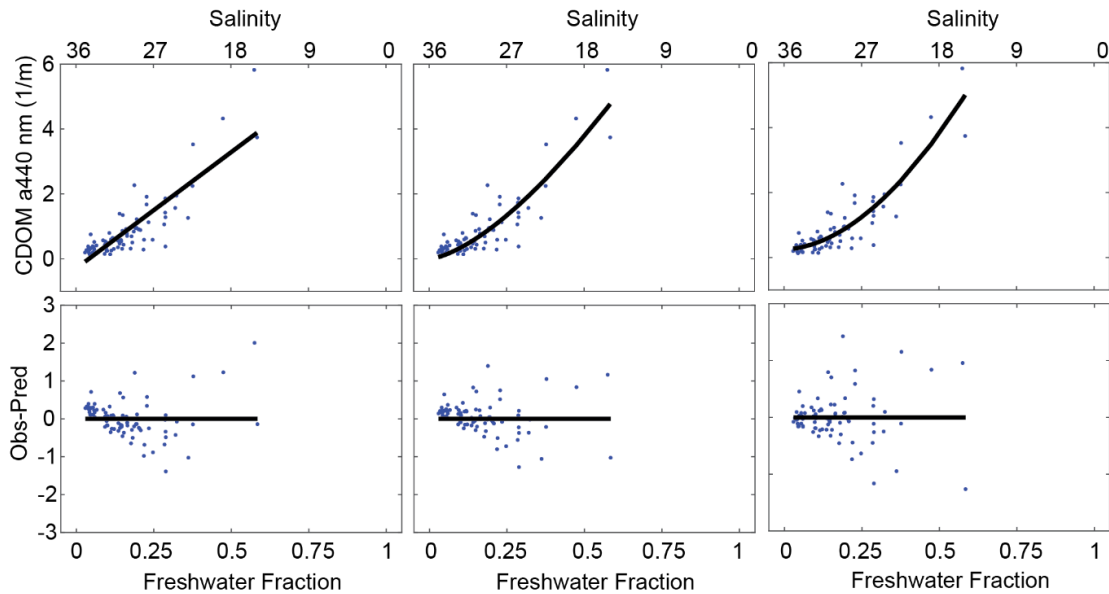
For the non-zero intercept power function, the best-fit intercept was positive, and its inclusion eliminated the tendency toward underestimation at higher salinities while also ensuring against negative CDOM estimates (Figure 8). The power function with a positive intercept explained 1% and 2% more of the variability in CDOM than the zero-intercept model for the Neuse and North Rivers, respectively, and the AICc scores indicated that it was superior among the three models (Table 3).

The positive intercept power function model is not only the best-fitting model, but also consistent with our understanding of the behavior of CDOM in estuaries and in the Neuse/Pamlico Sound in particular. Although CDOM can be degraded by sunlight and bacteria in estuaries, the degradation rates are generally slow enough that CDOM can be effectively considered a conservative property (Bowers and Brett 2008). Under ideal conditions of constant freshwater and seawater CDOM concentration and negligible degradation or production in the estuary, CDOM would exhibit a perfectly linear mixing curve when plotted against salinity (Loder et al. 1982). There could be several interacting processes that drive the observed concave-negative relationship between CDOM and salinity in the Neuse River Estuary (Figure 8). First, it is obvious from the high degree of scatter at low-salinity values that the freshwater CDOM concentration is not constant. When the time scales of variability in freshwater CDOM approximate the flushing time of an estuary, non-linear relationships between a conservative tracer and salinity can be produced (Loder and Reichard 1981); Bowers and Brett 2008). This seems likely to occur in the Neuse River estuary where both flushing time and CDOM concentration are tightly linked to river discharge (Hounshell et al. 2019). Second, the degree to which CDOM degradation influences CDOM concentration in an estuary is dependent on how much time CDOM spends in an estuary which is determined by the estuary's flushing time. The Neuse River Estuary has a flushing time that averages two months (Peierls et al. 2012). With such a long residence time, detecting the concave signature of CDOM degradation is more likely than in estuaries that are more rapidly flushed (Bowers and Brett 2008).
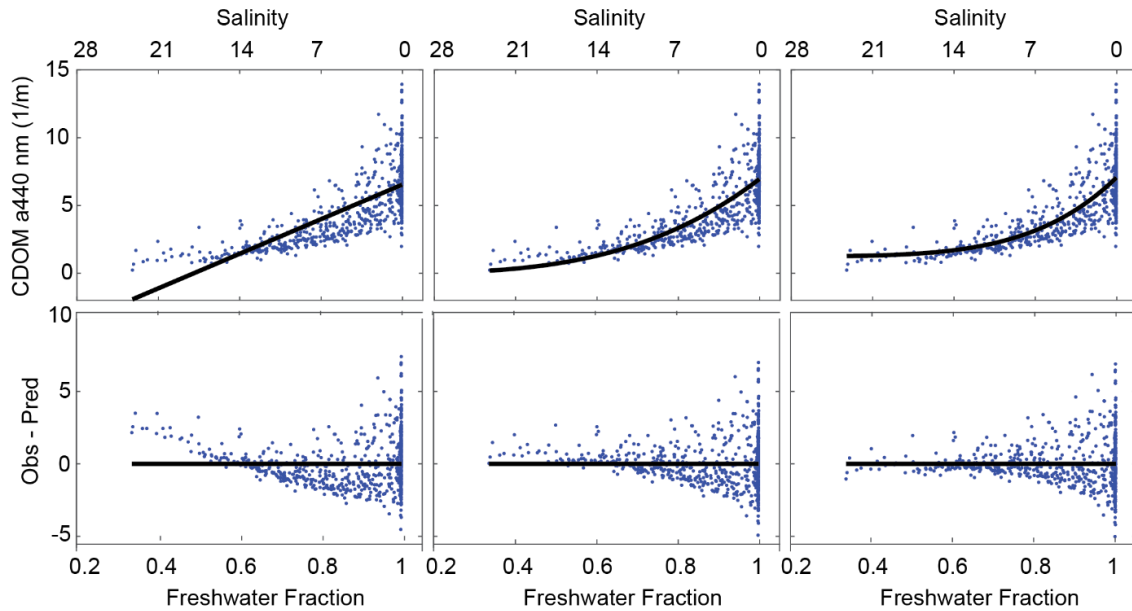
Figure 8. Empirical relationships between salinity (expressed as freshwater fraction) and CDOM in the Neuse River (ModMon data) and North River (Biber et al. 2008) using a linear regression model (left panels), a zero-intercept power function (middle panels) and a non-zero intercept power function (right panels). Solid lines in top panels are the best fit model. Solid black lines in the bottom panels indicate the zero line for comparison against model residuals (Observed-Predicted).

Generally, CDOM concentrations of seawater are considered negligible (Bowers and Brett 2008), but the best fit model for the Neuse River Estuary specified a moderate CDOM concentration at seawater salinity. Enclosed bays like North Carolina's sounds may have unusually high CDOM concentrations at near full seawater salinity (Bowers and Brett 2008). Due to the large surface area and shallow depths of North

Carolina's sounds, evaporation is an important component of their water budget accounting for about 20% of water losses from Pamlico Sound (Giese et al. 1979). Since evaporation increases the concentrations of dissolved substances, it could lead to measurable CDOM at a seawater salinity in Pamlico Sound even if seawater outside Pamlico Sound has negligible CDOM levels.

Despite being the superior model, the predictive capability of the model declined as the average CDOM concentration increased in fresher waters (Figure 8). Thus, our ability to estimate CDOM with the best-fit, positive-intercept power function model declines substantially for areas of the estuary where absorption by CDOM is most important in determining PAR attenuation. A high degree of error in the salinity/CDOM relationship at low salinities is consistent with the substantial variability of the CDOM concentration of incoming freshwater to the Neuse River Estuary created by different flow paths to the river (Hounshell et al. 2019). Under low, base-flow conditions river flow is dominated by low CDOM containing ground water, while under high flow conditions, overland runoff and flooding of wetlands contributes to higher CDOM (Hounshell et al. 2019). Since the positive-intercept power function model based on freshwater fraction explained a large amount of the variation in CDOM for both the Neuse River and North River estuaries, was relatively unbiased throughout the observed salinity ranges of the estuaries, and is consistent with our understanding of the fate and transport of CDOM in estuaries, this model was selected as a base model upon which the effects of other explanatory variables were tested in an effort to further improve the accuracy of CDOM estimates.

A fourth empirical model was developed that built on the positive-intercept power function model to include a term that captures the effect of variability in freshwater inputs on CDOM (Table 3). Accumulated antecedent rainfall for Hyde County prior to sample collection was chosen as a proxy of freshwater input. This decision to use Hyde County rainfall rather than gaged inputs was made based on several considerations. Flow to most estuarine waters in North Carolina is not gaged. Flow that is gaged is generally the portion above the fall line where wetlands that contribute substantial CDOM loads are inconsequential. Therefore, it is unlikely that gaged flows would be a strong predictor of CDOM loading. Precipitation should be a strong predictor of those coastal plain flows (Qi et al. 2009). Hyde County is central to the APES region and fortuitously has three rain gage sites that have been in operation for more than 20 years: site USC00312940 Fairfield, site USC00316349 Ocracoke, and site USC00318450 at the Swanquarter ferry landing.

Daily rainfall totals for the three stations were averaged to determine a daily average for the region and regional antecedent rainfall totals were calculated for each CDOM sample collection date. The appropriate antecedent rainfall accumulation period was chosen based on testing different accumulation periods from one day to half year for the Neuse River dataset where the variability in the freshwater end member was greatest, and thus the greatest need for correction existed. The model fit improved linearly

from a 1- to ~30-day accumulation period beyond which it slowly decreased (Figure 9). Consequently, a 30-day accumulated rainfall was chosen to represent recent freshwater inputs to the estuaries.
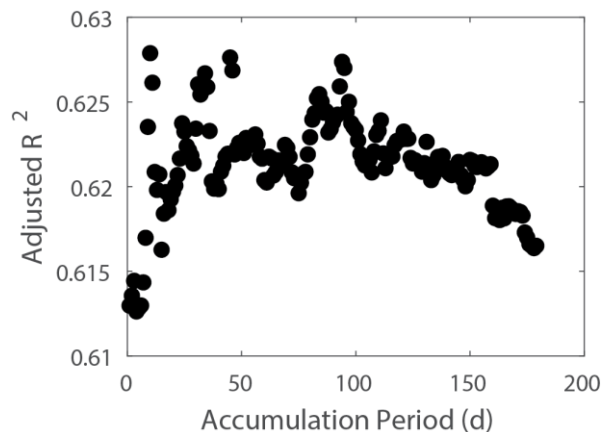

Figure 9. Adjusted R^2 values for the fit of CDOM by an empirical model with a power function of salinity (freshwater fraction) and a linear term for antecedent rainfall across different accumulation periods (see model in Table 3).

For the Neuse River, residuals from the positive-intercept power function model based on freshwater fraction also indicated that there was a modest degree of seasonality with a tendency toward higher CDOM concentrations during the warmest months of summer and early fall and lower CDOM during the coldest months of winter and early spring (Figure 10). Data from the North River were also consistent with this seasonality but there were no data collected during the summer and early fall (Figure 11) when CDOM reached its peak in the Neuse River. This seasonality with peak CDOM during summer is consistent with enhanced CDOM production by degradation of terrestrial plant matter in forest and wetland soils under warmer soil conditions (Wen et al. 2020) and seems likely to contribute seasonality to CDOM across North Carolina estuaries. Seasonality was added to a fifth candidate empirical model and was described as a sine function of the fraction of the year (fraction = 0 on 1 January and fraction = 1 on 31 December) of the sampling date (Table 3). As a final, sixth candidate empirical model, both rainfall and seasonality terms were added to the positive-intercept power function model.

Adding antecedent rainfall as a predictor did not improve model fit for the North River (Table 3). For the Neuse River, the AICc score showed that the model containing rainfall was superior to the base model but adding antecedent rainfall only explained an additional 1% of the CDOM variance (Table 3). Adding a seasonality term significantly improved the model, increasing the adjusted R^2 from 0.61 to 0.66 for the Neuse River (Table 3) and weakly improved model accuracy for the North River increasing the adjusted R^2 from 0.81 to 0.82 (Table 3). For both the Neuse and North Rivers, AICc scores indicated that models including seasonality were superior to models with no seasonal term. For the Neuse River, the best model included both seasonality and rainfall, while for the North River the best model included seasonality but not rainfall. For both rivers, the weights associated with the AICc scores indicated that there was no clear superiority of models that contained only a seasonal term versus models that contained both rainfall and seasonality. Without strong evidence for including antecedent rainfall, and with an aim of keeping the model as simple as possible, the final models selected for both the Neuse River and North River were the positive-intercept power function models based on freshwater fraction with a seasonal term.
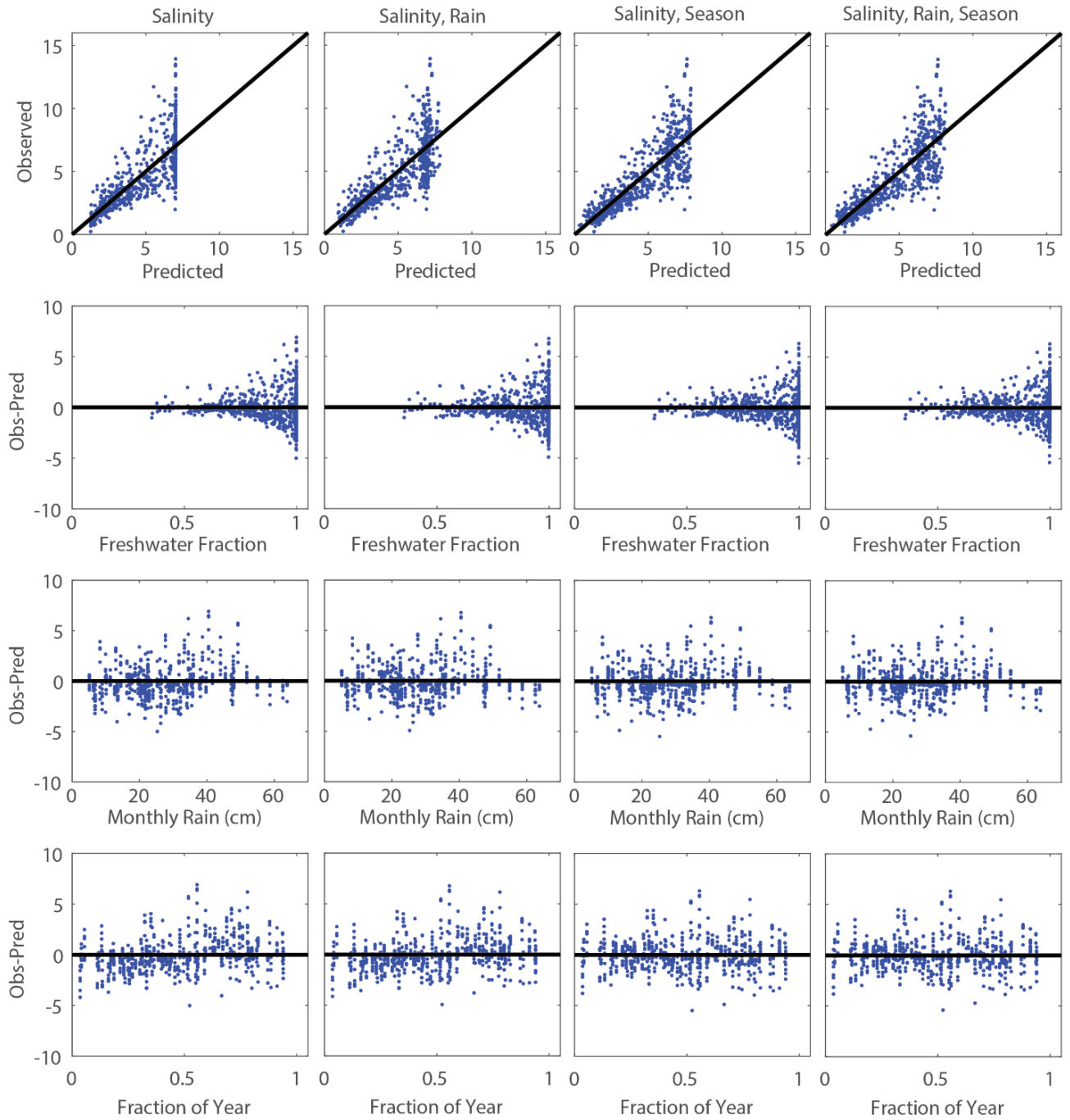
Figure 10. Model residuals versus freshwater fraction, monthly rain totals, and seasonality for the Neuse River dataset. Residuals were calculated as observed CDOM minus predicted CDOM for models (labeled above each column of panels) that included combinations of freshwater fraction, antecedent monthly rainfall totals, and seasonality.
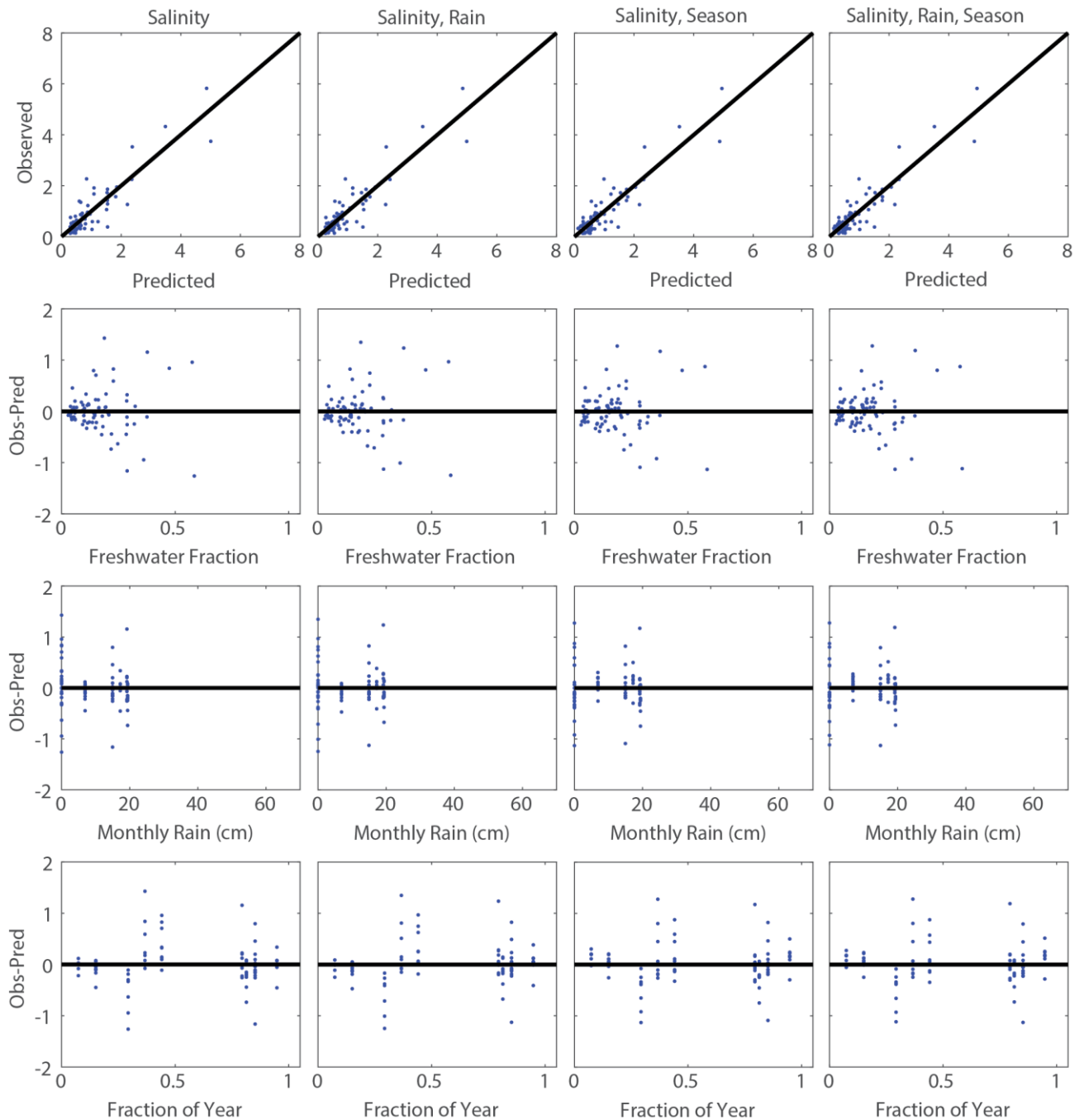
Figure 11. Model residuals versus freshwater fraction, monthly rain totals, and seasonality for the North River dataset. Residuals were calculated as observed CDOM minus predicted CDOM for models (labeled above each column of panels) that included combinations of freshwater fraction, antecedent monthly rainfall totals, and seasonality.

Both the empirical model of CDOM developed for the Neuse and North Rivers were compared against direct measurements of CDOM from Pamlico Sound that were made during this study (Figure 12). The empirical model of CDOM derived from the North River overestimated

Pamlico Sound CDOM by a factor of ~6 at the lowest observed concentrations and ~2 at the highest concentrations. The model derived from the Neuse River dataset provided much more accurate estimates, with the highest observed values underpredicted by ~20% and the lowest observed values overestimated by about a factor of 2. These results indicate that the salinity and seasonal influences on CDOM concentration are system specific, and likely linked to differences in freshwater CDOM loading that arise from land use, particularly percent wetland cover, within different watersheds (Spencer et al. 2013). The ability of the Neuse River empirical model to more accurately estimate southwestern Pamlico Sound CDOM likely results from the Neuse River being the major source of freshwater (Jia and Li 2012), and also likely CDOM, to southwestern Pamlico Sound.
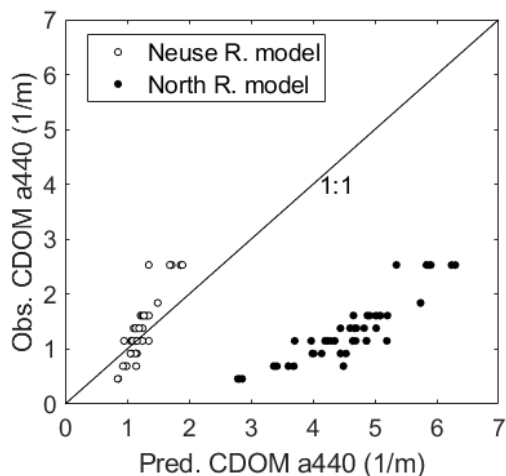
Figure 12. Comparison of directly measured Pamlico Sound CDOM concentration versus estimated CDOM derived from empirical relationships with salinity and season observed in the Neuse River and North River estuaries.

As a hybrid piedmont/coastal plain river, the Neuse River is more like the large low-salinity SAV zones in Albemarle Sound and Pamlico River than is the North River. For this reason, CDOM estimates of the low-salinity SAV zones were made using the empirical models derived from the Neuse River dataset. Such use of an empirical CDOM model to estimate CDOM for waters that are not directly connected to where the model was developed may produce unquantified error and/or bias in the CDOM estimates that will impact the ability to accurately estimate K_{dPAR} using the bio-optical model. For high-salinity waters where CDOM plays a less important role in PAR attenuation, the CDOM model used (either Neuse River or North River model) was chosen based on the degree of hydrological connectivity between that water body and either the Neuse River or North River. The model derived from the North River dataset was used to estimate CDOM for Core, Back, and Bogue Sounds while the Neuse River model was used to estimate CDOM for Pamlico Sound.

5.3. Bio-optical model validation (Objective 3)

Linear regression models were used to characterize the model fit between observed and predicted K_{dPAR} values (Figure 13). These regression models, being empirically based, only provide a convenient way for expressing the predictive capability and biases of the model and provide no information on the mechanisms behind the optical model's performance. As expected, the bio-optical model accurately predicted the observed K_{dPAR} for the North River dataset upon which the model was calibrated (Figure 13). A regression of predicted versus observed K_{dPAR} had a slope near unity (0.97), an intercept near zero

(0.08 m^{-1}) and a modestly strong R^2 value (R^2 = 0.67) (Figure 13). Consistent with the slope and intercept, the model had minimal bias with mean and median underestimation of K$_{dPAR}$ of less than 0.05 m^{-1} (Table 6). Although this result was expected, it is included here for comparison against the validation results from other water bodies and because it was not included in the original paper (Biber et al. 2008).

Table 6. Bio-optical model validation by comparison of observed K$_{dPAR}$ with K$_{dPAR}$ calculated via the bio-optical model for North Carolina estuaries.

Water Body	Sample number	Mean (Median) Obs K$_{dPAR}$ (m^{-1})	Mean (Median) Pred. K$_{dPAR}$ (m^{-1})	RMSE (m^{-1})	Mean (Median) Bias (Obs-Pred) (m^{-1})	Mean (Median) Bias Ratio (Obs/Pred)
North River	85	1.12 (1.01)	1.07 (1.01)	0.27	0.05 (0.04)	1.05 (1.04)
Bogue Sound	297	1.27 (1.12)	0.94 (0.87)	0.56	0.34 (0.27)	1.40 (1.35)
Pamlico Sound (2000-2020) (CDOM estimated)	1009	0.99 (0.91)	0.73 (0.68)	0.35	0.27 (0.25)	1.40 (1.36)
Pamlico Sound 2020 (CDOM measured)	45	1.18 (1.24)	0.71 (0.69)	0.50	0.47 (0.48)	1.66 (1.70)
Pamlico Sound 2020 (CDOM estimated)	45	1.18 (1.24)	0.76 (0.78)	0.46	0.41 (0.43)	1.55 (1.57)
Neuse River	503	1.99 (1.98)	1.31 (1.31)	0.81	0.68 (0.65)	1.53 (1.52)
Neuse River (salinity<1)	244	2.42 (2.32)	1.53 (1.48)	0.97	0.89 (0.80)	1.58 (1.54)
Neuse River (salinity 1-5)	138	2.19 (2.09)	1.44 (1.35)	0.87	0.75 (0.73)	1.55 (1.55)
Neuse River (salinity >5)	121	1.69 (1.59)	1.18 (1.11)	0.63	0.51 (0.54)	1.50 (1.49)
Albemarle Sound	436	2.06 (1.96)	1.36 (1.30)	0.82	0.70 (0.67)	1.53 (1.53)
Pamlico River	572	1.91 (1.92)	1.26 (1.31)	0.69	0.62 (0.60)	1.52 (1.52)
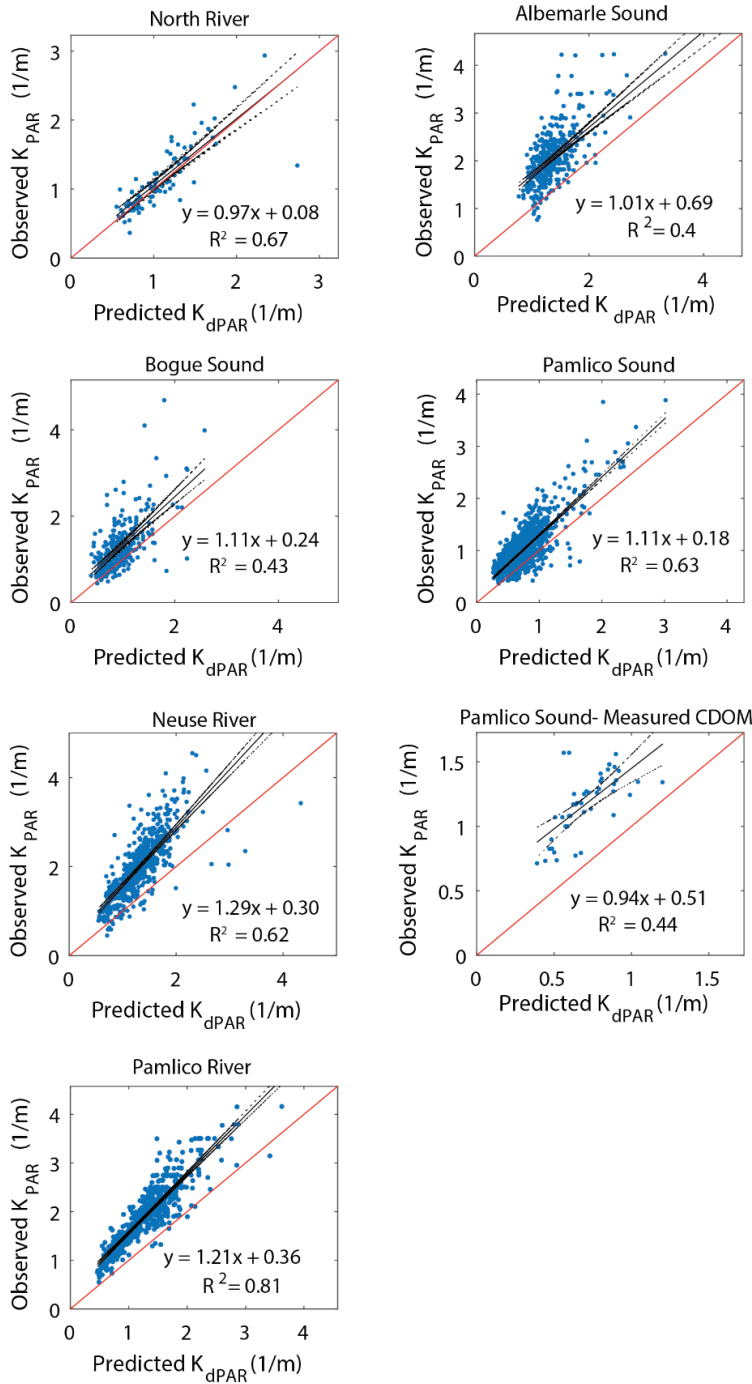
Figure 13. Comparison of observed K_{dPAR} to predictions of K_{dPAR} from the bio-optical model for high- and low-salinity waters throughout APES. Blue dots represent individual observations and predictions. Black solid lines represent a linear regression model of observed on predicted values with equation and correlation coefficient provided. Dotted black lines represent the 95% confidence interval on the regression and the solid red line indicates the reference (1:1) line.

For Bogue Sound, the model did not perform as well as for the North River. The regression of predicted versus observed K_{dPAR} had a slope slightly higher than unity (1.11) and a positive intercept (0.24) that

combined to produce a modest underestimation of the actual observed K_{dPAR} (Figure 13) with mean and median biases of 0.34 and 0.27 m^{-1} (Table 6). The strength of the relationship ($R^2 = 0.43$) was also significantly weaker than for the North River. For the Neuse River, the relationship between observed and predicted K_{dPAR} was modestly strong ($R^2 = 0.62$) but with a slope of 1.29 and intercept of 0.30, the model underestimated K_{dPAR} by about 50% (Figure 13, Table 6). With a slope of about 1.2 and an intercept of 0.36, the model fit to K_{dPAR} estimates for Pamlico River was similar to the fit for the Neuse River. RMSE error, mean absolute error, mean bias ratio (Table 6) and the R^2 value ($R^2 = 0.81$) from the regression of predicted vs. observed values all indicated that the bio-optical model predictions for Pamlico River fit observations slightly better than for the Neuse River. This was surprising since errors in estimating K_{dPAR} from SD for the Pamlico River dataset should add significantly to the error in the bio-optical model validation.

For Albemarle Sound and its tributaries, the bio-optical model significantly underpredicted K_{dPAR} across the range of K_{dPAR} values as shown by the slope near one but a large (0.69) intercept for the regression of predicted on observed K_{dPAR} values. Compared to the Pamlico River and Neuse River, there was a larger scatter in the relationship between bio-optical model predictions and observed K_{dPAR} that may stem from a combination of a poorer ability to estimate K_{dPAR} from SD (Table 2) or CDOM from salinity, or from a greater diversity of optical characteristics within the particulate fraction across such a large system that receives water from diverse watershed types.

For Pamlico Sound, when CDOM was estimated based on the empirical model derived from the Neuse River, both the slope (1.11) and intercept (0.18) of the relationship of observed versus predicted K_{dPAR} indicated a closer model fit to observations compared to the results from the Neuse River, Pamlico River or Albemarle Sound (Figure 13). On average the model underestimated K_{dPAR} in southwest Pamlico Sound by approximately 40% (Table 3). Using direct measurements of CDOM collected from June to December 2020 to estimate K_{dPAR} for Pamlico Sound did not improve the model fit. In fact, the bias worsened, and the model underestimated K_{dPAR} by ~70%. Incorrect estimation of CDOM is clearly not the main source of the model bias for Pamlico Sound or for the Neuse River where CDOM was directly measured for all samples. The bias in K_{dPAR} estimates for the Neuse River was explored further by breaking the samples into groups by salinity. Both the absolute and relative model biases were most severe in freshwater samples (salinity < 1) and progressively lessened in groupings of oligohaline (salinity 1-5) and mesohaline waters (salinity 5-23) (Figure 14, Table 6).
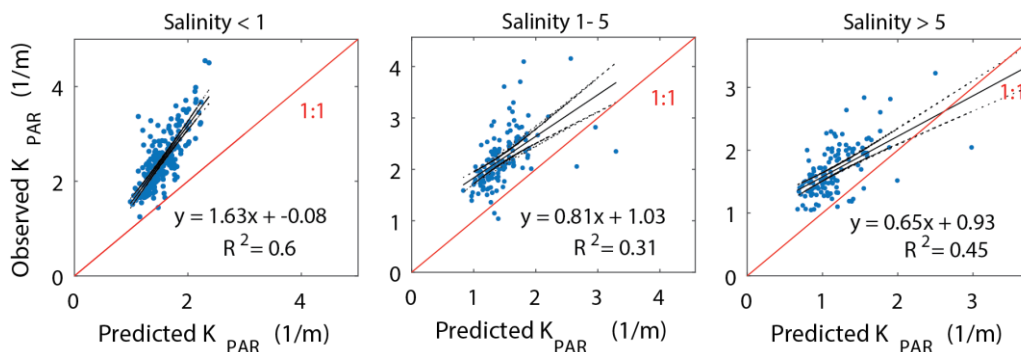

Figure 14. Comparison of observed K_{dPAR} to predictions of K_{dPAR} from the bio-optical model along the salinity gradient in the Neuse River Estuary. Blue dots represent individual observations and predictions. Black solid lines represent a linear regression model of observed on predicted values with equation and correlation coefficient provided. Dotted black lines represent the 95% confidence interval on the regression and the solid red line indicates the reference (1:1) line.

Although there was hope that the Biber et al. (2008) bio-optical model would serve equally-well across the APES, these validation results indicate that the model performs best for high-salinity waters near the North River where it was originally calibrated. The underprediction of K_{dPAR} in Albemarle Sound, Pamlico River, and Neuse River along with the increasingly severe underprediction bias of K_{dPAR} along the salinity gradient from Pamlico Sound to the upper Neuse River estuary is an indication that the model is incorrectly parameterized for some aspect(s) of the absorption and/or scattering properties of optically active constituents associated with freshwater inputs to the APES. Reducing the bias will require recalibrating the bio-optical model for low-salinity waters that appear optically distinct from the North River. Resulting improvements in K_{dPAR} estimates will greatly increase confidence in the model's ability to accurately determine Chl*a* thresholds for meeting the low-salinity water clarity target. Despite the severe bias, there was still a tight linear relationship (just far from the 1:1 line) between observed and modeled K_{dPAR} in low-salinity waters. This tight linear relationship suggests that the model has a high likelihood of providing accurate and precise K_{dPAR} estimates once it has been properly recalibrated.

5.4. Chl*a* thresholds for high- and low-salinity SAV zones (Objective 4)

Across the nine datasets from high-salinity waterbodies (see Figure 15 for locations), Chl*a* thresholds that maintained K_{dPAR} at or below 0.89 m^{-1} ranged from 0-36 µg L^{-1}- and averaged 15 µg L^{-1} (Figure 16, Table 7). The analyses also revealed important roles for CDOM and turbidity in PAR attenuation of the high-salinity SAV zones. In these plots, the line of constant attenuation equal to the water clarity target is expressed as a function of Chl*a* and turbidity, water quality properties that are manageable through watershed nutrient and sediment load reductions (Gallegos et al. 2001). Although CDOM does not appear on the axes of these plots, its influence can be clearly seen in the line of constant PAR attenuation as differences in distance from the origin. For example, the x-intercept, where K_{dPAR} is controlled only by CDOM and Chl*a* varied from 42 µg L^{-1} in the relatively CDOM-rich southwestern part of Pamlico Sound to 76 µg L^{-1} in the CDOM-poor waters at Shackleford Banks (Figure 16). The influence of turbidity combined with CDOM on PAR attenuation was especially strong in the upper North River and caused K_{dPAR} to exceed 0.89 m^{-1} even in the complete absence of Chl*a*. For many of the areas (Lower North River, Bogue Sound, Core Sound, Pamlico Sound at Ocracoke and Pamlico Sound near the Outer Banks) turbidity was the primary contributor of PAR attenuation, and median turbidity levels placed the average K_{dPAR} close to the water clarity target even in the absence of Chl*a* (Figure 16).
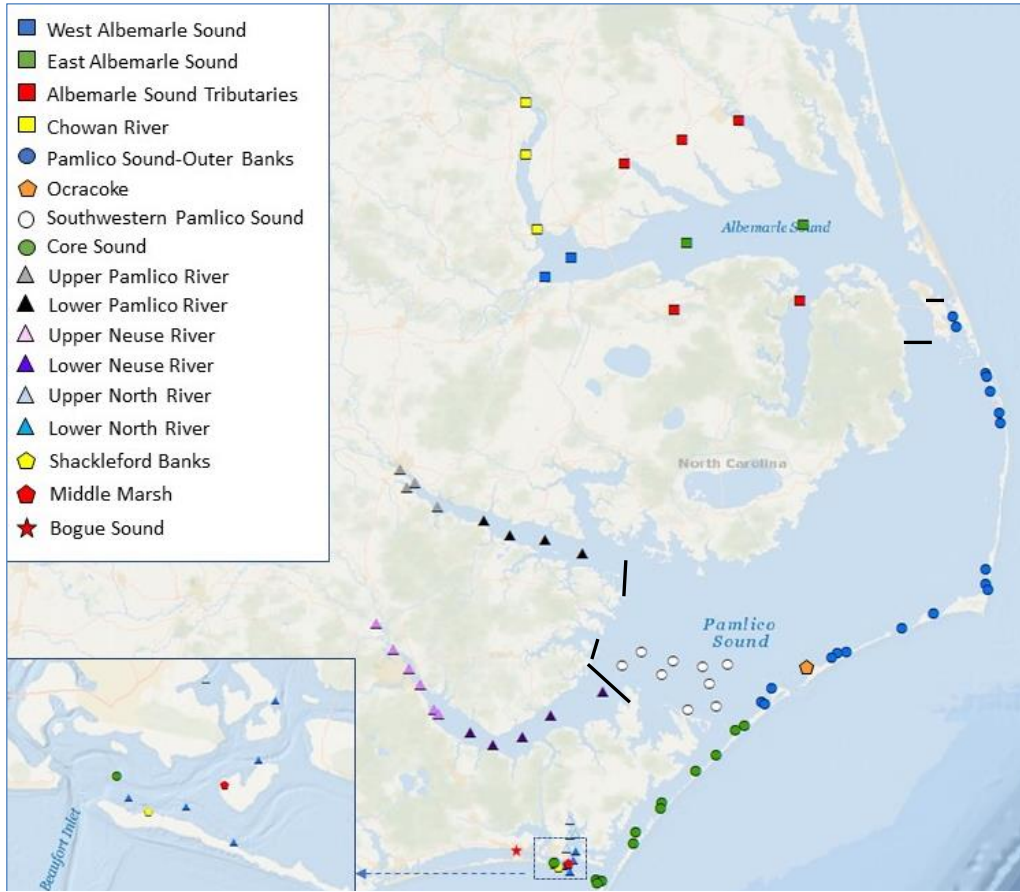
Figure 15. Map of the stations contained within the datasets used to establish high- and low-salinity Chl*a* thresholds using the bio-optical model. Waters upstream of dark lines including Albemarle and Currituck Sounds, and the Pamlico, Neuse and Bay Rivers were considered low-salinity estuaries. Further clarification of characterization of high- and low-salinity zones can be found in Table 7.
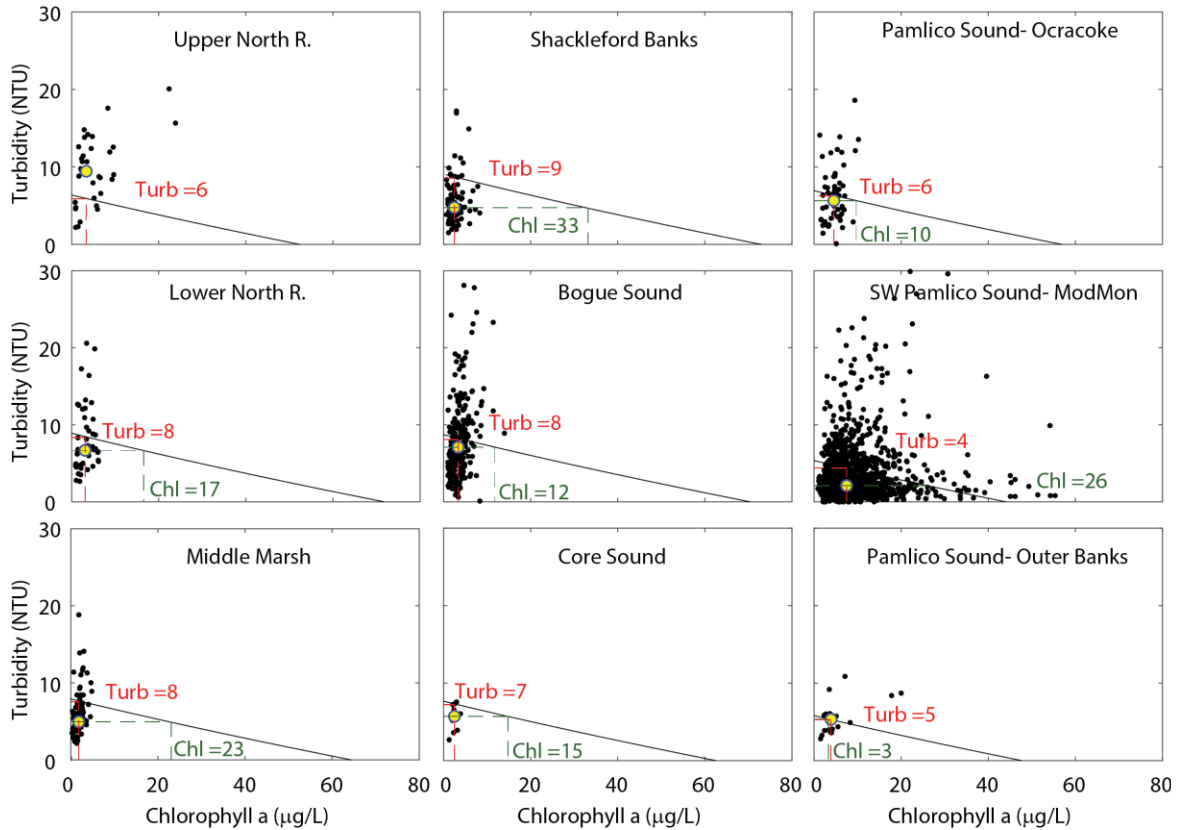
Figure 16. Light threshold model applied to data from high-salinity waters within APES. Solid line indicates the line of constant attenuation ($K_{dPAR} = 0.89$ m^{-1}) at the high-salinity PAR attenuation target. Solid black dots represent measured turbidity and Chl*a* values from each waterbody, and large yellow dots indicate median turbidity and Chl*a* values. Dashed green lines link median turbidity to the maximum Chl*a* threshold above which the PAR attenuation target is exceeded. Dashed red lines link median Chl*a* to the maximum turbidity threshold above which the PAR attenuation target is exceeded. See Figure 15 for locations of the water bodies and sampling stations.

The Chl*a* threshold for Shackleford Banks (33 µg L^{-1}) was greater than for all other sites and was the only site that had a threshold Chl*a* greater than 30 µg L^{-1} (Figure 16, Table 7). At a Chl*a* level of 23 µg L^{-1} Middle Marsh had the third highest Chl*a* threshold. Both Shackleford Banks and Middle Marsh are close to Beaufort Inlet, and therefore are more strongly influenced by dilution of optical constituents with high clarity ocean waters. For the other high-salinity areas, the North River, Bogue Sound, Pamlico Sound, and Core Sound, high levels of background turbidity, and to a lesser extent CDOM, led to much lower Chl*a* thresholds ranging from 0 to 26 µg L^{-1}, and an average threshold of 12 µg L^{-1}. The threshold for southwest Pamlico Sound, 26 µg L^{-1}, was the highest of the seven areas that were not immediately inside Beaufort Inlet (i.e., stations other than Middle Marsh and Shackleford Banks).

The higher Chl*a* threshold for southwest Pamlico Sound was due to median turbidity levels that were less than half that of the other areas, including the nearshore SAV habitats of Pamlico Sound on the back barrier shelf behind the Outer Banks (Figure 16, Table 7), and also partly due to the underestimation bias that became more severe in these relatively lower-salinity waters (Table 7). Lower turbidity in the deeper waters of Pamlico Sound may result from reduced susceptibility of resuspension from waves and currents and dilution of resuspended sediments in the larger volume associated with deeper waters. Alternatively, lower turbidity measured in the deeper portions of Pamlico Sound may be due to a bias toward sampling

the open waters of Pamlico Sound on less-windy, calmer days when sediment resuspension is lessened. Higher turbidity at the two shallow-water datasets from behind the Outer Banks in Pamlico Sound (the routine monitoring at Ocracoke and a synoptic survey during July 2015 from Bodie Island to Shackleford Banks both conducted by the Cape Hatteras National Seashore - see Table 1) led to lower Chl*a* thresholds of 10 µg L^{-1} at Ocracoke and 3 µg L^{-1} from Bodie Island to Shackleford Banks. The lower Chl*a* thresholds indicated by data collected in the shallower, nearshore areas are therefore most appropriate for evaluating the current North Carolina standard and establishing new statewide or regional Chl*a* standards for protecting SAV habitats. This finding also suggests that use of deep-water monitoring locations for establishing shallow-water optical conditions may underestimate PAR attenuation within shallow water SAV habitats, particularly where turbidity is a major component of PAR attenuation.

Turbidity thresholds identified by the inverted bio-optical model for high-salinity waters ranged from 4 to 9 NTU. Across the nine high-salinity datasets, higher CDOM and moderate Chl*a* levels resulted in the lowest turbidity thresholds, 4-6 NTU all occurring in Pamlico Sound. A threshold turbidity value of 5 NTU is appropriate to meet the light requirements of Pamlico Sound which represents the majority of NC's high salinity SAV habitat area.

Table 7. Modeled Chl*a* thresholds for protection of SAV and median values of optical indicators in high- and low-salinity regions of APES.

Salinity Zone	Location	Median CDOM a_{440} (1/m)	Median Chl *a* (µg/L)	Chl *a* Threshold (µg/L) (95% C.I.)	Median Turbidity (NTU)	Turbidity Threshold (NTU) (95% C.I.)
High	Upper North River	1.01	3.4	[2]0	9.4	5.9 (5.0-6.9)
High	Lower North River	0.34	3.1	17 (8-22)	6.7	8.3 (7.8-8.7)
High	Middle Marsh	[1]0.59	1.8	23 (14-28)	4.9	7.6 (7.5-7.7)
High	Shackleford Banks	[1]0.31	2.5	33 (24-37)	4.8	8.5 (8.2-8.9)
High	Bogue Sound	[1]0.39	3.4	12 (7-19)	7.1	8.1 (8.1-8.3)
High	Core Sound near Outer Banks	[1]0.65	2.5	15 (3-22)	5.7	7.2 (5.7-7.5)
High	Pamlico Sound at Ocracoke	[1]0.79	4.5	10 (4-19)	5.7	6.3 (5.6-6.9)
High	Southwestern Pamlico Sound	[1]1.33	7.5	26 (25-28)	2.1	4.4 (4.3-4.8)
High	Pamlico S. near Outer Banks	[1]1.19	3.9	3 (0-16)	5.3	5.3 (5.1-5.6)
Low	Western Albemarle Sound	[1]6.69	7.6	[2]0	6.1	1.7 (1.7-2.1)
Low	Eastern Albemarle Sound	[1]4.72	12.0	7 (6-12)	5.3	4.6 (4.4-5.3)
Low	Chowan River	[1]6.80	5.5	[2]0	5.6	1.8 (1.6-2.4)
Low	Albemarle Tributaries	[1]6.04	7.7	[2]0	5.7	2.8 (2.7-3.5)
Low	Upper Pamlico River	[1]5.23	23.0	[2]0	7.6	2.1 (1.4-2.7)
Low	Lower Pamlico River	[1]1.76	14.0	76 (72-77)	3.5	10.6 (10.3-10.8)
Low	Upper Neuse River	6.25	10.4	[2]0	5.8	2.1 (2.0-2.4)
Low	Lower Neuse River	2.08	17.1	77 (76-78)	2.5	9.5 (9.3-9.6)
[1]CDOM values were estimated by empirical relations with salinity and season described in section 3.2. [2]Median turbidity and CDOM caused K_{dPAR} to exceed the Chl*a* threshold even if Chl*a* was zero.						

A threshold of approximately 15 µg L^{-1} Chl*a* appears appropriate to meet the light requirements for high-salinity SAV habitats of Core and Bogue Sounds. This value, 15 µg L^{-1} Chl*a*, is the same Chl*a* threshold established for polyhaline regions of Chesapeake Bay based on the presence/absence of SAV beds (Dennison et al. 1993). The thresholds from the two datasets available for the SAV area in Pamlico Sound along the Outer Banks provided Chl*a* thresholds of 10 µg L^{-1} for the time series at Ocracoke and 3 µg L^{-1} for the SECN synoptic survey. These thresholds are lower than for the other high-salinity areas and suggest that perhaps the threshold for these areas may need to be lower. However, these thresholds were

calculated based on a very small amount of data which leads to high uncertainty. It seems particularly likely that the small snapshot of conditions captured by the SECN synoptic survey failed to adequately define the average turbidity and CDOM concentrations of this large area and there is low confidence in the very low 3 µg L^{-1} threshold calculated for this region. The 95% confidence intervals for the Chl*a* thresholds from both datasets overlapped a Chl*a* value of 15 ug L^{-1} which is consistent with 15 ug L^{-1} being a threshold broadly protective of high-salinity SAV zones in North Carolina.

Chl*a* and turbidity thresholds were calculated for eight low-salinity regions within the APES. Of these regions, only the lower segment of the Neuse and Pamlico Rivers and eastern Albemarle Sound had a Chl*a* threshold greater than zero (Figure 17, Table 7). For all other regions, the combination of CDOM and turbidity produced PAR attenuation that exceeded the low-salinity water clarity target even in the absence of Chl*a*. For eastern Albemarle Sound, the model calculated a low Chl*a* threshold of 7 µg L^{-1}, and at 12 µg L^{-1}, median Chl*a* was nearly twice this threshold. In contrast, Chl*a* thresholds for the lower Neuse and Pamlico Rivers were 77 and 76 µg L^{-1}, respectively, and median Chl*a* values were much lower than the thresholds at 14 and 17 µg L^{-1}, respectively. Median turbidity for the lower regions of the Neuse and Pamlico Rivers was very low (< 3 NTU) and CDOM a$_{440}$ was moderate at ~ 2 m^{-1} (Table 7).
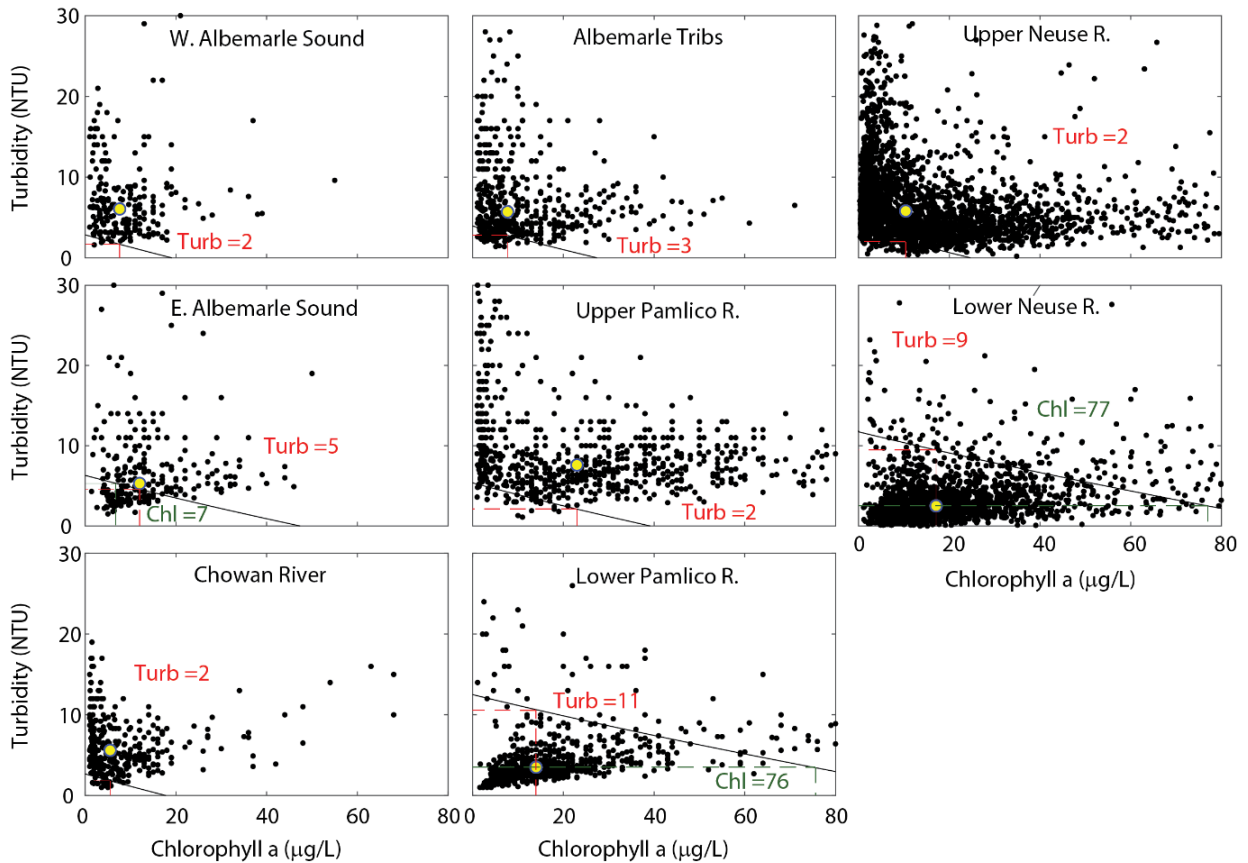
Figure 17. Light threshold model applied to data from low-salinity waters within APES. Solid line indicates the line of constant attenuation (K$_{dPAR}$ = 1.36 m^{-1}) at the low-salinity PAR attenuation target. Solid black dots represent measured turbidity and Chl*a* values from each waterbody, and large yellow dots indicate median turbidity and Chl*a* values. Dashed green lines link median turbidity to the maximum Chl*a* threshold above which the PAR attenuation target is exceeded. Dashed red lines link median Chl*a* to the maximum turbidity threshold above which the PAR attenuation target is exceeded. See Figure 15 for locations of the water bodies and sampling stations.

45

Similarly, the combination of high CDOM and Chl*a* generally led to much lower turbidity thresholds compared to the turbidity thresholds of the high-salinity estuarine waters (Figure 17, Table 7). The tributaries and western part of Albemarle Sound and the upper parts of the Neuse and Pamlico Rivers had low turbidity thresholds within the narrow range of 2-3 NTU. The turbidity threshold in eastern Albemarle Sound was slightly higher at 5 NTU. Within all of these regions, median turbidity was much higher than the turbidity threshold. In contrast, the lower CDOM and Chl*a* levels of the lower Neuse and Pamlico Rivers produced relatively high turbidity thresholds of ~10 NTU, and in these areas median turbidity is significantly less than the turbidity threshold for low-salinity SAV.

Although it appears that the Chl*a* and turbidity thresholds for the lower parts of the Neuse and Pamlico Rivers are much higher than the current levels of Chl*a* and turbidity, the estimates of PAR attenuation for all of these low-salinity estuarine zones are underestimates. Therefore, all of the low-salinity thresholds should be considered overestimates and the true low-salinity zone Chl*a* and turbidity thresholds are likely lower by an amount approximated by the underestimation of K_{dPAR}, ~50% for the Neuse and Pamlico Rivers (Table 7). Determining scientifically defensible Chl*a* and turbidity thresholds for low-salinity waters will require recalibrating the bio-optical model to account for the optical differences of the suspended particulate material of the different low-salinity waterbodies.

5.5. Comparison of Chl*a* and turbidity thresholds for SAV to water quality standards (Objective 5)

Based on the underlying distributions of Chl*a* within North Carolina estuarine waters, a scatter plot of median vs. 90th quantiles for Chl*a* (Figure 18) showed that a median value of 15 μg L^{-1} corresponds closely to a 90th quantile of 40 μg L^{-1}. Therefore, in the absence of statistical uncertainty, the current Chl*a* standard of 40 μg L^{-1} set at the 90th quantile and the 15 μg L^{-1} threshold calculated for high-salinity regions of Core Sound south and west through Bogue Sound are basically equivalent, and the standard as it is currently written would be protective for these high-salinity SAV habitats as long as a high enough number of samples is collected to make uncertainty negligible. In practice, smaller sample size generated considerable uncertainty. A scatter plot of median Chl*a* versus Chl*a* at the critical quantile for a declaration of impairment (i.e., listing on the US EPA's 303d list of impaired waters) (Figure 18) showed that the median threshold value of 15 μg L^{-1} determined by the bio-optical model as protective for high-salinity regions of Core Sound south and west through Bogue Sound corresponds to a critical value of Chl*a* of about 30 μg L^{-1}, approximately 25% lower than the current Chl*a* standard of 40 μg L^{-1} set at the 90th quantile. The analysis was also applied to determine what Chl*a* standard assessed using the current methodology and sampling frequency would be required if a lower threshold of 10 μg L^{-1} was deemed necessary for the protection of Pamlico Sound's SAV beds along the Outer Banks. Results indicated that a standard of about 20 μg L^{-1} Chl*a* would be protective of a 10 μg L^{-1} median Chl*a* threshold using current sampling frequency and statistical assessment methodology.

The median turbidity threshold value of 5 NTU determined by the bio-optical model as protective for high-salinity SAV zones corresponds to a 90th quantile of 12 NTU, less than half the current standard of 25 NTU. When statistical uncertainty is considered, a median turbidity threshold of 5 NTU corresponded to a critical value of turbidity of about 10 NTU. So, with current assessment methods, the current turbidity standard of 25 NTU would need to be reduced to 10 NTU to protect a median turbidity of 5 NTU or less.

Clearly, the current Chl*a* and turbidity standards combined with the current assessment methodology and uncertainty related to sample size result in impairment assessments that do not provide an adequate degree of protection of water clarity for high-salinity SAV. For Chl*a*, assessments based on larger sample sizes could reduce statistical uncertainty and result in an assessment approach that is protective of high-salinity SAV without changing the current numeric standard. For turbidity, however, the current 25 NTU

standard is at least a factor of 2 too high, and the numeric standard will need to be lowered significantly to protect high salinity SAV.

5.6. Comparison of current water clarity to SAV-related water clarity targets (Objective 6)

Direct measurements, model predictions from the bio-optical model, and estimates of K_{dPAR} based on SD measurements were compared for high- and low-salinity waters throughout APES against the high- and low-salinity SAV zone targets for PAR transmission, 22 and 13 % of incident PAR to 1.7 and 1.5 m depth, respectively. Recall that these water clarity targets were derived based on a compilation of SAV light requirements for growth and empirical observations about the colonization depths of SAV for high- and low-salinity regions of North Carolina's estuarine waters.

In general, water clarity in Albemarle Sound and its tributaries does not meet low-salinity SAV light requirements. The western most areas of the Albemarle Sound system, including the Chowan River and near the mouth of the Roanoke River had the greatest water clarity with many sites having PAR availability greater than half the target (Figure 19). Eastward, water clarity of Albemarle Sound and its tributaries including the Scuppernong, Alligator, Perquimans, Little, Pasquotank and North Rivers was poorer, with most sites achieving less than 25% of the targeted PAR availability. Water clarity met the target at five sites in Albemarle Sound. At these sites, K_{dPAR} was directly measured as part of the NCCA and the validity of the data is not questioned. However, only one or at most two measurements were made at each site, and it appears likely that the measurements were made during a period of unusually good water clarity not representative of the average condition. This trend of spatially coherent patterns of water clarity with a few outliers represented by stations with low sample number was common throughout the APES. Water clarity in Currituck Sound increased from north to south with PAR attenuation in the northern part north of the Narrows generally achieving less than 25% of the PAR target, and water clarity south of the Narrows achieving 25-50% of the target.
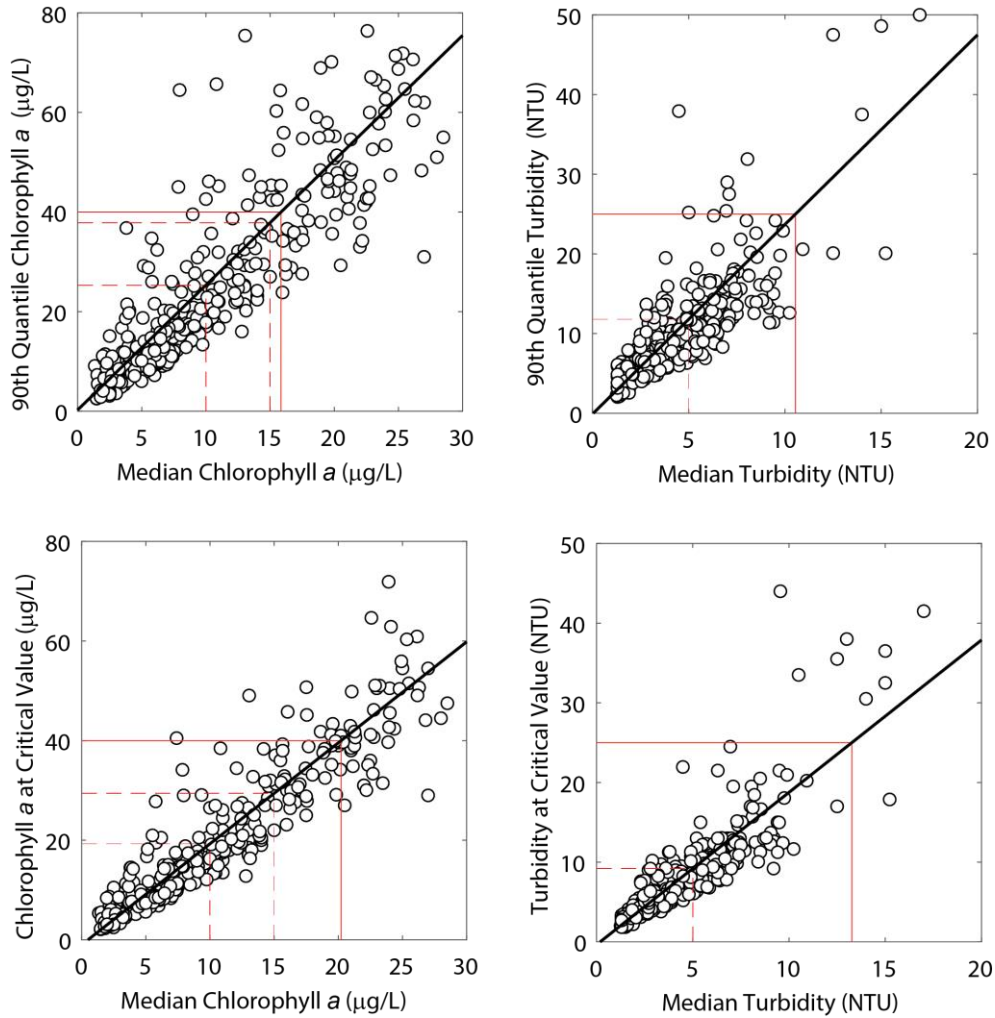
Figure 18. Scatter plot of median Chl*a* (left panels) and turbidity (right panels) versus values at the 90th quantiles (top panels) and at the critical quantiles for a 303d listing as an impaired water (bottom panels) for monitoring locations throughout North Carolina estuarine waters. Red dashed lines link Chl*a* and turbidity thresholds identified by the bio-optical model for high-salinity SAV waters to the equivalent Chl*a* and turbidity values at critical quantiles used for assessing impairment. Red solid lines link median Chl*a* and turbidity to the current NC numeric standards for Chl*a* and turbidity as they are assessed using current sampling frequency and statistical methodologies.
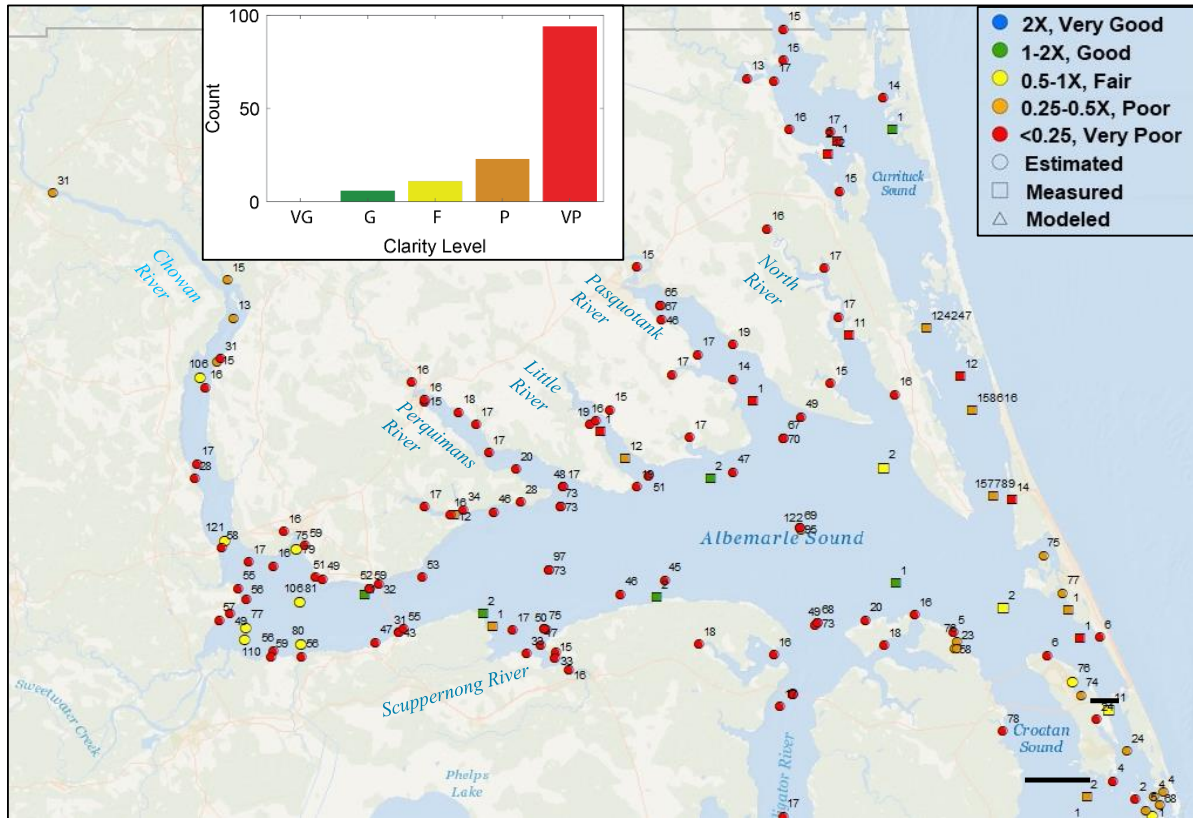
Figure 19. Map of Albemarle and Currituck Sounds showing light availability for SAV. Symbol colors indicate PAR availability expressed as the fraction of the low-salinity SAV PAR target (13% incident PAR to 1.5 m depth). Symbol shapes represent whether K_{dPAR} at the station were estimated from Secchi disk measurements, directly measured using a PAR sensor, or modeled via the bio-optical model. Small numbers beside each symbol indicate the number of K_{dPAR} values from each station. Percentage cut offs for each category include the lower end and exclude the upper end of the range. Inset histogram shows the distribution of clarity levels within the area of interest delineated by solid black lines.

Water clarity in the high-salinity waters of Pamlico Sound also exhibited coherent patterns with strong east to west and north to south gradients (Figure 20). Along the western side of Pamlico Sound, PAR availability was almost always less than 50% of the high-salinity target. Clarity at sites on the western shore of Pamlico Sound from Wysocking Bay north generally had clarity that provided less than 25% of the PAR target while clarity in western shore areas south and west of Wysocking Bay typically provided 25-50% of the target. At most Pamlico Sound stations between Pamlico River and Bay River, PAR availability was fair, achieving 50-100% of the target. The open waters of southwestern Pamlico Sound that were largely assessed by direct measurements made at nine stations by the ModMon program had water clarity that was slightly less than the target with all the ModMon stations except one having clarity 50-100% of the target. The other ModMon station north of Cedar Island met the target and three sites directly measured by the NCCA program showed a range of values from meeting the target to less than 25% of SAV PAR target. Along the shallow eastern side of Pamlico Sound where most of North Carolina's SAV occurs, water clarity was very near the target with most sites achieving 50-200% of the clarity target. The area north of Oregon Inlet was an exception where PAR availability at most stations was less than 50% of the target.
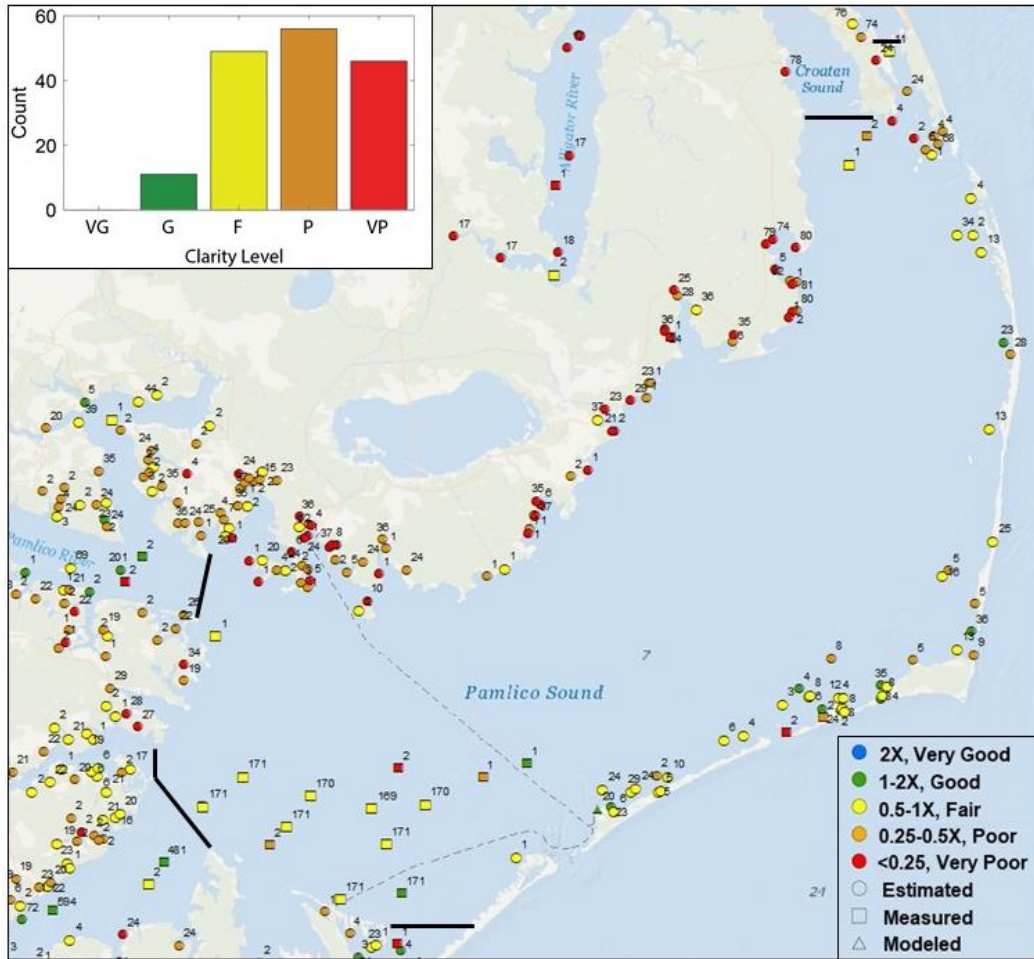
Figure 20. Map of Pamlico Sound showing light availability for SAV. Symbol colors indicate PAR availability expressed as the fraction of the high salinity SAV PAR target (22% incident PAR to 1.7 m depth). Symbol shapes represent whether K_{dPAR} at the station were estimated from Secchi disc measurements, directly measured using a PAR sensor, or modeled via the bio-optical model. Small numbers beside each symbol indicate the number of K_{dPAR} values from each station. Percentage cut offs for each category include the lower end and exclude the upper end of the range. Inset histogram shows the distribution of clarity levels within the area of interest delineated by solid black lines.

Low-salinity waters of Pamlico and Pungo Rivers and their tributaries generally had clarity that did not meet the low-salinity PAR availability target (Figure 21). A downstream gradient of improving clarity was apparent within the Pamlico River where waters upstream of the Aurora ferry crossing (dashed line in Figure 21) generally had clarity that provided less than 50% of the PAR target while waters downstream including the Pungo River provided PAR closer (50-100%) to the target. Most open water stations of the downstream Pamlico River and stations near creek mouths had sufficient clarity to meet the PAR target. Clarity within some of the tributary creeks such as South Creek and Goose Creek exhibit downstream

50

gradients similar to the main stem Pamlico River with poorer clarity upstream.
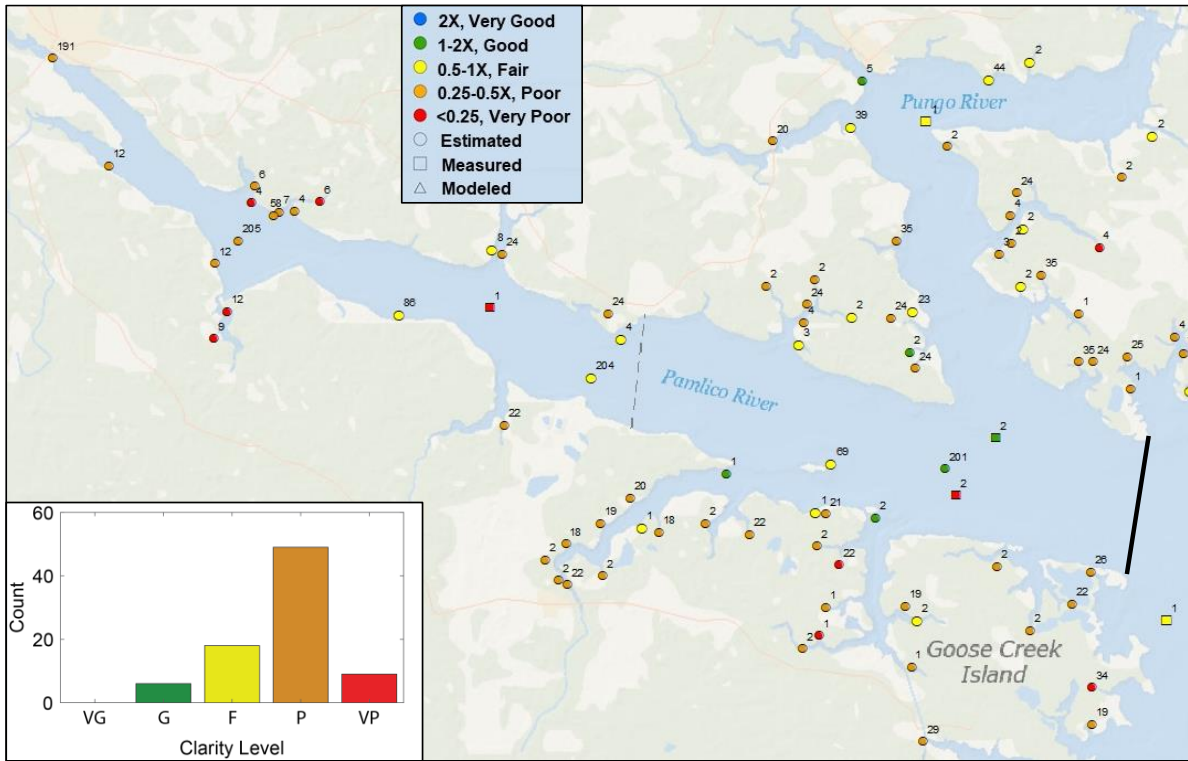
Figure 21. Map of the Pamlico and Pungo Rivers showing light availability for SAV. Symbol colors indicate PAR availability expressed as the fraction of the low-salinity SAV PAR target (13% incident PAR to 1.5 m depth). Symbol shapes represent whether K_{dPAR} at the station were estimated from Secchi disk measurements, directly measured using a PAR sensor, or modeled via the bio-optical model. Small numbers beside each symbol indicate the number of K_{dPAR} values from each station. Percentage cut offs for each category include the lower end and exclude the upper end of the range. Inset histogram shows the distribution of clarity levels within the area of interest delineated by the solid black line. Dashed line represents the Aurora ferry crossing.

A similar downstream gradient was observed in the Neuse River (Figure 22). Stations upstream of Fairfield harbor where the estuary widens generally provided less than 50% of the PAR target. Stations from Fairfield to Cherry Branch where the estuary bends toward the northeast, generally achieved 50-100% of the target, and from there downstream, the open waters of the Neuse River met the water clarity target. Tributary creeks generally had lower clarity and generally achieved less than 50% of the PAR target. Most stations on the Bay River achieved 50-100% of the low-salinity PAR target with a few stations achieving less but no stations meeting the clarity target (Figure 22).
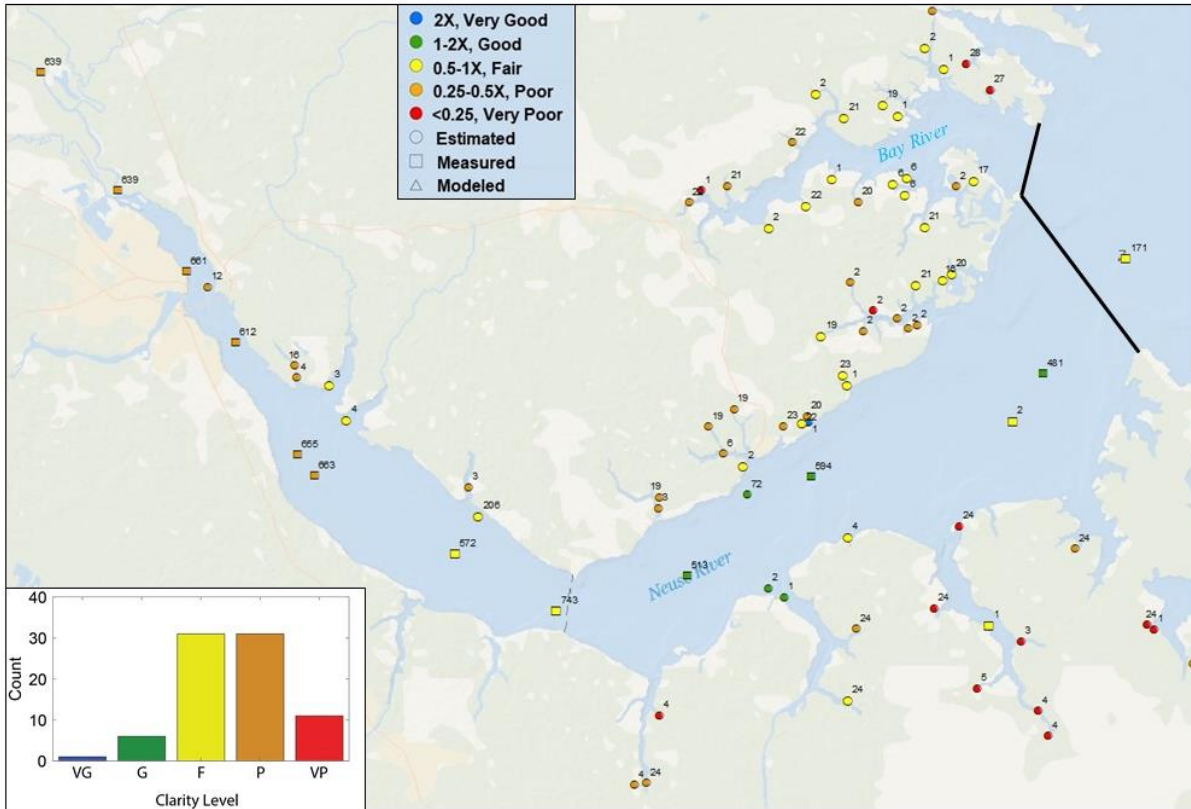
Figure 22. Map of the Neuse and Bay Rivers showing light availability for SAV. Symbol colors indicate PAR availability expressed as the fraction of the low-salinity SAV PAR target (13% incident PAR to 1.5 m depth). Symbol shapes represent whether K_{dPAR} at the station were estimated from Secchi disk measurements, directly measured using a PAR sensor, or modeled via the bio-optical model. Small numbers beside each symbol indicate the number of K_{dPAR} values from each station. Percentage cut offs for each category include the lower end and exclude the upper end of the range. Inset histogram shows the distribution of clarity levels within the area of interest delineated by solid black lines.

Of all the waters within APES, Core Sound has the best water clarity (Figure 23). Nearly half of the sites within Core Sound met the high-salinity PAR attenuation target, and five stations achieved twice the targeted PAR availability. Water clarity in tributary creeks along the western margin of Core Sound was highly variable achieving from less than half to more than 100% of the PAR target (Figure 23). Within Back Sound and North River, sites near Beaufort Inlet are generally meeting the high-salinity water-clarity target while stations further inland generally achieve 50-100% of the PAR target (Figure 23). Some of the tributary creeks of the North River and the upper Newport River have poorer clarity that provide only 25-50% of the PAR target. The large dataset of direct K_{dPAR} measurements made by UNC-IMS off its dock indicate that the clarity target is not being met at this site (64% of the target). PAR attenuation estimates derived from SD generally indicate that water-clarity targets are met in Bogue Sound (100-200% of the target) (Figure 24) but most of these sites are in tributary creeks that empty to Bogue Sound and may not represent clarity in the main body of Bogue Sound. Median clarity at the single
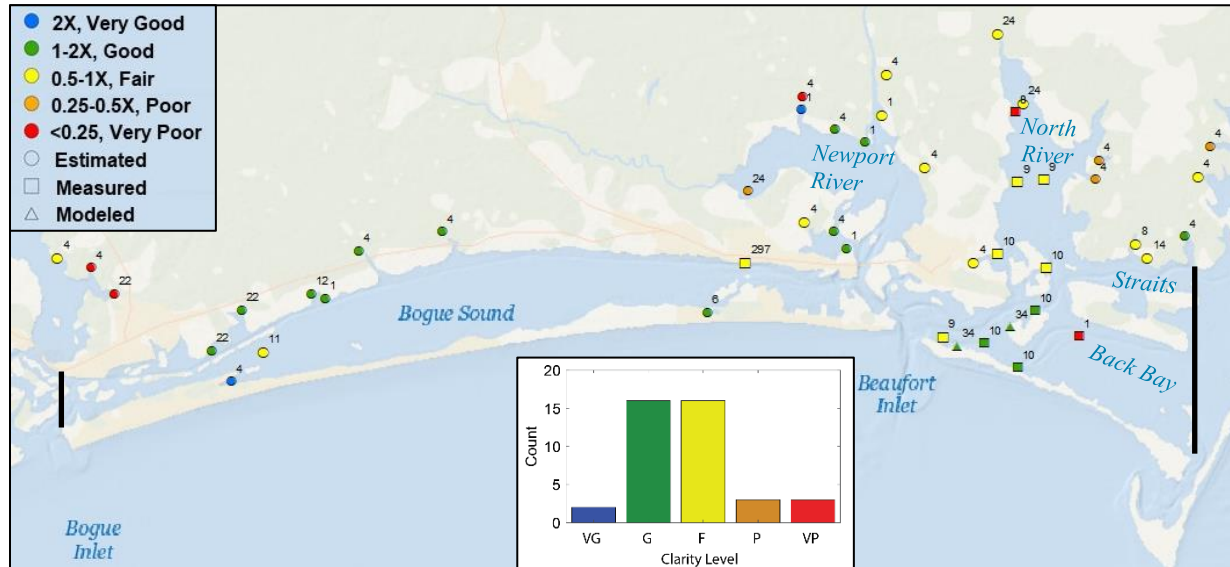
station in the main body of western Bogue Sound was 98% of the PAR target.
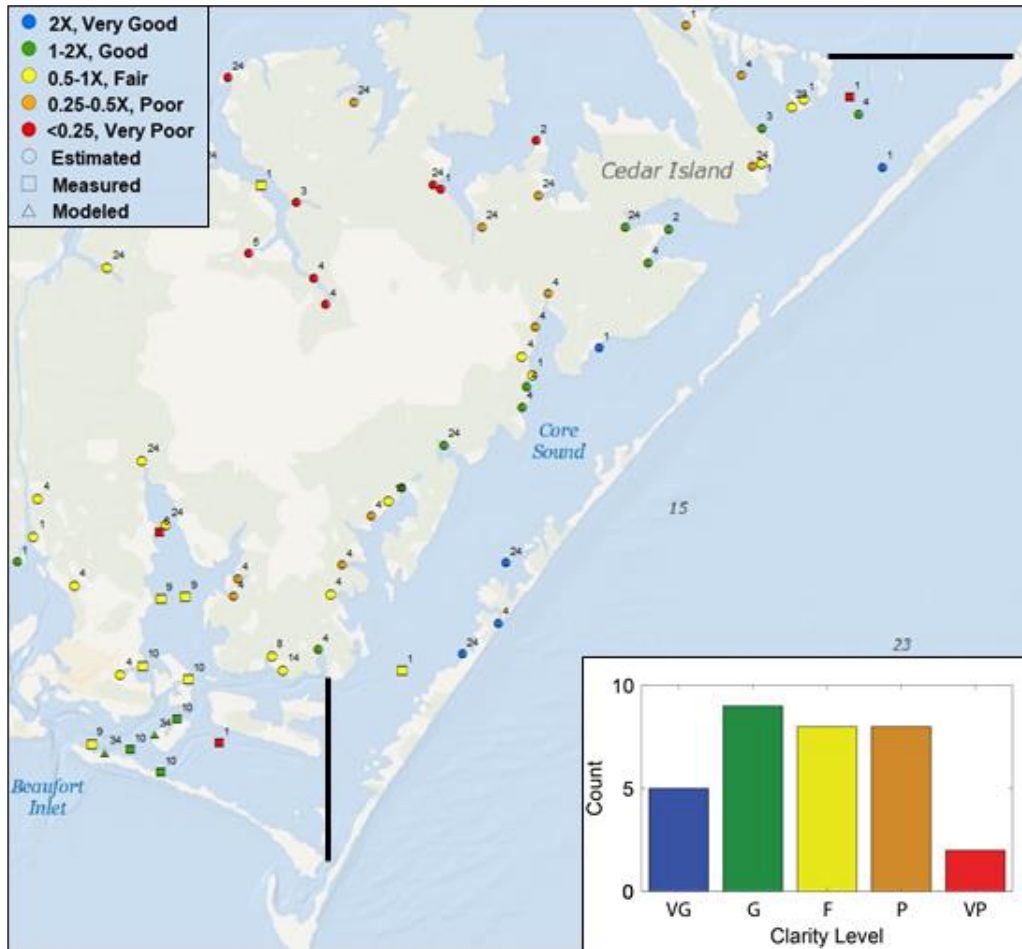
Figure 23. Map of Core Sound showing light availability for SAV. Symbol colors indicate PAR availability expressed as the fraction of the high-salinity SAV PAR target (22% incident PAR to 1.7 m depth). Symbol shapes represent whether K_{dPAR} at the station were estimated from Secchi disk measurements, directly measured using a PAR sensor, or modeled via the bio-optical model. Small numbers beside each symbol indicate the number of K_{dPAR} values from each station. Percentage cut offs for each category include the lower end and exclude the upper end of the range. Inset histogram shows the distribution of clarity levels within the area of interest delineated by solid black lines.

Between aerial surveys of SAV coverage conducted by APNEP in 2006-2007 and 2013, the area between Barden's Inlet and Bogue Inlet experienced an 11% decline in SAV coverage. The decline in this southern region of APES was greater than declines observed for northern and central regions of the APES and has been putatively linked to the relatively higher and growing population density of the area, particularly for western Bogue Sound where SAV declines were highest (Field et al. 2021). However, the analysis of water clarity presented here shows that, on average, PAR attenuation of western Bogue Sound should be favorable for the persistence of SAV. It is important to remember that K_{dPAR} conditions shown here are median values over the past 20 years. Examining the time course of K_{dPAR} estimates for the two longest records from western Bogue Sound revealed that K_{dPAR} increased (water clarity declined) from below the PAR attenuation target to above the target at about the time of the 2013 survey, and then decreased again (improved water clarity) to below the target in 2019. In eastern Bogue Sound, K_{dPAR} exhibited a slight decline over the same period (Figure 25). Whether the increase in K_{dPAR} in western

Bogue Sound was the cause of the observed decline in SAV coverage is unclear but it does highlight the possibility that substantial changes in water clarity may have occurred during the 20-year averaging period used in this study, and that the average PAR attenuation may not accurately reflect current conditions. An examination of variation in trends over time in K_{dPAR} throughout APES was outside the scope of this project but would significantly improve our understanding of the status and trajectory of changing light conditions for SAV within the APES.

Figure 24. Map of Bogue Sound showing light availability for SAV. Symbol colors indicate PAR availability expressed as the fraction of the high-salinity SAV PAR target (22% incident PAR to 1.7 m depth). Symbol shapes represent whether K_{dPAR} at the station were estimated from Secchi disk measurements, directly measured using a PAR sensor, or modeled via the bio-optical model. Small numbers beside each symbol indicate the number of K_{dPAR} values from each station. Percentage cut offs for each category include the lower end and exclude the upper end of the range. Inset histogram shows the distribution of clarity levels within the area of interest delineated by solid black lines.
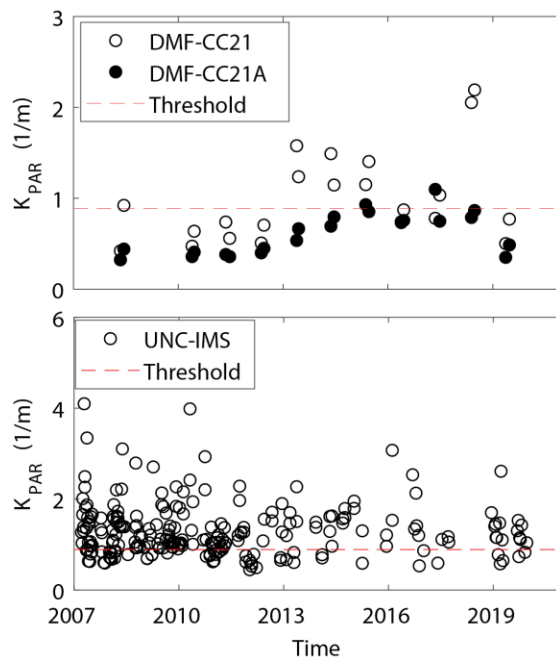
Figure 25. Time series of K_{dPAR} estimates derived from Secchi disk depth data collected by NCDMF at two stations in western Bogue Sound and direct K_{dPAR} measurements by UNC-IMS at the UNC-IMS dock in eastern Bogue Sound (yellow square with sample number equal to 297 in Figure 24). The NCDMF stations correspond to the green circles with sample numbers equal to 22 shown in Figure 24. CC21 is to the northeast of CC21A. The dashed red line indicates the high-salinity K_{dPAR} target for high-salinity waters, 0.89/m.

6. Data Gaps (Objective 7)

6.1. CDOM data

CDOM is an important component of light absorption throughout North Carolina estuarine waters and can be the dominant component in low-salinity zones (Woodruff et al. 1999; Corbett et al. 2020). It is also the least routinely measured of the three optically active constituents required to model PAR attenuation and accurately determine impacts of additional attenuation due to changes in Chl$a$. The only CDOM datasets currently available are from the Neuse River and North River estuaries. However, there are opportunities to expand the availability of CDOM data without significant expense. A plan is currently being developed to collect CDOM for the Albemarle Sound and Pamlico Rivers in conjunction with NCDWR's AMS monitoring. This will produce the coincident turbidity, Chl$a$, and CDOM data necessary to predict K_{dPAR} from the bio-optical model. There are also remote sensing techniques developed for use across several platforms (e.g., Landsat, ETM+, OLCI, etc.) that could be exploited to hind cast CDOM concentrations based on nearly three decades of satellite imagery (Griffin et al. 2018). Additionally, the USACE has collected a valuable, high temporal resolution (15-minute), long-term (three-year) CDOM dataset for two sites in Currituck Sound. This dataset is currently expressed as arbitrary fluorescence units and would require post-calibration by paired measurements of Currituck water samples using the CDOM fluorescence instrument and a spectrophotometer to measure absorbance at 440 nm. This post-calibration exercise should receive high priority, as it would produce an extensive optical dataset for assessing SAV habitat conditions and the factors that control the dynamics of water clarity in Currituck Sound, historically the largest low-salinity SAV habitat in North Carolina (NCDEQ 2021a).

6.2. Direct measurements of K_{dPAR}

Like CDOM, direct measurements of K_{dPAR} are scarce for APES. Long-term records are restricted to the Neuse River, southwest Pamlico Sound, and the dock at UNC-IMS on Bogue Sound. Although, as demonstrated in this project, SD can be used to estimate K_{dPAR}, there is always an increased level of uncertainty in the estimates, particularly when the estimates are made for regions hydrologically distinct from the waters where the empirical models used to relate SD and K_{dPAR} were developed. Adding direct measures of K_{dPAR} to current monitoring programs such as the AMS, or the Cape Hatteras/Cape Lookout National Seashore's monitoring programs that already measure SD could provide valuable K_{dPAR} data that could be used directly to understand water clarity in important SAV zones but could also be used to develop improved region-specific empirical models to relate SD to K_{dPAR}.

6.3. Measurements of optically active water quality constituents from SAV habitats along the Outer Banks

The water-clarity information for Pamlico Sound and Core Sounds along the Outer Banks primarily consists of SD collected by NCDMF. Data on turbidity, Chl$a$, and CDOM to determine the drivers of PAR attenuation for this important high-salinity SAV habitat are available only from one long-term monitoring station at Ocracoke, sampling of a few stations once every five years as part of the NCCA, and a single synoptic survey of 18 stations conducted by Cape Hatteras/Cape Lookout National Seashore's monitoring program as part of the SECN. The concentrations of optically active constituents in the nearshore, shallow SAV beds differ substantially from the deeper areas of Pamlico Sound monitored by ModMon. So, determining the drivers of water clarity for North Carolina's most expansive SAV habitats would be greatly improved by more data collected from within waters over the SAV beds. Establishing routine monitoring of optical properties at several sentinel sites along the Outer Banks should be a priority and would improve confidence in Chl$a$ threshold concentrations for the expansive SAV habitats on the back barrier shelves behind the Outer Banks. Monitoring of optical constituents is

more frequent along the southern Outer Banks, particularly near Beaufort Inlet where the NERRS in collaboration with Cape Hatteras/Cape Lookout National Seashore maintains two continuous monitoring stations at Middle Marsh and Shackleford Banks, and UNC-IMS conducts the Bogue Watch program in eastern Bogue Sound. These monitoring programs should be supported to ensure continued data availability for this area where human population and coastal development pressures are high, and the decline in high-salinity SAV acreage is steepest among APNEP's survey regions (Field et al. 2021).

6.4. Measurements of the scattering and absorption spectra and scaling coefficients for low-salinity SAV zones

The bio-optical model clearly performed better for high-salinity waters than for low-salinity waters where it consistently underpredicted observed K_{dPAR}. Each of the model coefficients shown in Table 5 as well as the spectral absorption shape function for phytoplankton were determined based on measurements of scattering and absorption of water samples collected along the estuarine gradient of the North River, a high-salinity, coastal plain estuary. Some of the model parameters, particularly the ratio of backscattering-to-scattering and turbidity-specific backscattering coefficient are extremely sensitive to the composition of suspended particulates in the water, and dominant particulate type can vary substantially between high- and low-salinity waters (Woodruff et al. 1999). Even the spectrum of CDOM changes as it is photodegraded during downstream transport in estuaries, resulting in an increase in spectral slope and changes in the ability to estimate CDOM absorption across the PAR wavelengths (400-700 nm) from CDOM measurements made at 440 nm (Gallegos et al. 2005). Accurately portraying the optical characteristics of CDOM, non-algal particulates, and phytoplankton within the low-salinity waters of APES will require recalibrating the bio-optical model for those waters. As mentioned previously, although the current model underestimates K_{dPAR}, there was still a strong relationship between model predictions and observed K_{dPAR} values. The strength of the relationships provide confidence that the model will be able to estimate K_{dPAR} with an acceptable degree of accuracy and precision once it is calibrated for the distinct scattering and absorbing properties of the optically active constituents of the low-salinity estuarine zones.

7. Acknowledgments

8. References

APNEP (Albemarle-Pamlico National Estuary Partnership). 2020. Clean Waters and SAV: Making the Connection Technical Workshop summary report. APNEP, 1601 Mail Service Center, Raleigh, NC https://apnep.nc.gov/our-work/monitoring/submerged-aquatic-vegetation-monitoring/clean-waters-and-sav-making-connection

Biber, P.D., Gallegos, C.L., Kenworthy, W.J. 2008. Calibration of a bio-optical model in the North River, North Carolina (Albemarle-Pamlico Sound): A tool to evaluate water quality impacts on seagrasses. *Estuaries and Coasts* 31: 177-191.

Bowers, D.G., Brett, H.L. 2008. Relationship between CDOM and salinity in estuaries: An analytical and graphical solution. *Journal of Marine Systems* 73: 1-7.

Corbett, D.R., Biarrieta, N., Dickhudt, P., Fonseca, M., Hodel, E., Mason, E., Paris, P., Wadman, H., Walsh, J.P. 2020. Final Report. SAVE Currituck Sound: Submerged aquatic vegetation evaluation in Currituck Sound, NC. NCDOT Project 2018-05.

Dennison, W.C., Orth, R.J., Moore, K.A., Stevenson, J.C., Carter, V., Kollar, S., Bergstrom, P.W., Batiuk, R.A. 1993. Assessing water quality with submerged aquatic vegetation. *Bioscience* 43: 86-94.

Fernandes, M.B., Daly, R., Van Gils, J., Kildea, T., Caires, S., Erftemeijer, P.L.A. 2018. Parameterization of an optical model to refine seagrass habitat requirements in an urbanized coastline. *Estuarine, Coastal and Shelf Science* 207: 471-482.

Field, D., Kenworthy, J., Carpenter, D. 2021. Extent of submerged aquatic vegetation: High salinity waters. Metric report. (REVISED). Albemarle-Pamlico National Estuary Partnership. Raleigh, NC. 19 pp. https://apnep.nc.gov/documents/files/metric-report-extent-submerged-aquatic-vegetation-high-salinity-estuarine-waters

Gallegos, C.L. 2001. Calculating optical water quality targets to restore and protect submerged aquatic vegetation: Overcoming problems in partitioning the diffuse attenuation coefficient for photosynthetically active radiation. *Estuaries* 24: 381-397.

Gallegos, C.L. 2005. Optical water quality of a blackwater river estuary: the Lower St. Johns River Florida, USA. *Estuarine, Coastal, and Shelf Science* 63: 57-72.

Gallegos, C.L., Werdell, P.J., McClain, C.R. 2011. Long-term changes in light scattering in Chesapeake Bay inferred from Secchi depth, light attenuation, and remote sensing measurements. *Journal of Geophysical Research-Oceans* 116: C00H08

Giese, G.L., Wilder, H.B., Parker, G.G. Jr . 1979. Hydrology of major estuaries and sounds of North Carolina. U.S. Geological Survey Water Resources Investigation 79-46: 1-175.

Griffin, C.G., McClelland, J.W., Frey, K.E., Fiske, G., Holmes, R.M. 2018. Quantifying CDOM and DOC in major Arctic rivers during ice-free conditions using Landsat TM and ETM+ data. *Remote Sensing of Environment* 209: 395-409.

Hall, M.J., Van den Boogaard, H.F.P., Fernando, R.C., Mynett, A.E., 2004. The construction of confidence intervals for frequency analysis using resampling techniques. *Hydrology and Earth System Sciences* 8, 235-246.

Hall, N.S., Paerl, H.W., Peierls, B.L., Whipple, A.C., Rossignol, K.L. 2013. Effects of climatic variability on phytoplankton biomass and community structure in the eutrophic, microtidal, New River Estuary, North Carolina, USA. *Estuarine and Coastal Shelf Science* 117: 70-82.

Harborne, A.R., Mumby, P.J., Fiorenza, M., Perry, C.T., Dahlgreen, C.P., Holmes, K.E., Brumbaugh, D.R. 2006. The functional value of Caribbean coral reef, seagrass and mangrove habitats to ecosystem processes. *Advances in Marine Biology* 50: 57-189.

Hounshell, A.G., Rudolph, J.C., Van Dam, B.R., Hall, N.S., Osburn, C.L., Paerl, H.W. 2019. Extreme weather events modulate processing and export of dissolved organic carbon in the Neuse River Estuary, NC. *Estuarine, Coastal and Shelf Science* 219: 189-200.

Jia, P., Li, M. 2012. Dynamics of wind-driven circulation in a shallow lagoon with strong horizontal density gradient. *Journal of Geophysical Research* 117; C05013, doi:10.1029/2011JC007475.

Kemp, W.M., Batiuk, R., Bartleson, R., Bergstrom, P., Carter, V., Gallegos, C.L., Hunley, W. Karrh, L,. Koch, E.W., Landwehr, J.M., Moore, K.A., Murray, L., Naylor, M., Rybicki, N.B., Stevenson, J.C., Wilcox, D.J. 2004. Habitat requirements for submerged aquatic vegetation in Chesapeake Bay: Water quality, light regime, and physical-chemical factors. *Estuaries* 27: 363-377.

Kirk, J.T.O. 1994. *Light and photosynthesis in aquatic ecosystems*. Cambridge University Press, Cambridge.

Lebo, M.E., Paerl, H.W., Peierls, B.L. 2012. Evaluation of progress in achieving TMDL mandated nitrogen reductions in the Neuse River Basin, North Carolina. *Environmental Management* 49: 253-266.

Lee, Z., Du, K., Arnone, R. 2005. A model for the diffuse attenuation coefficient of downwelling irradiance. *Journal of Geophysical Research* 110: C02016, doi: 10. 1029/2004JC002275, 2005.

Lefcheck, J.S., Wilcox, D.J., Murphy, R.R., Marion, S.R, Orth, R.J. 2017. Multiple stressors threaten the imperiled coastal foundation species eelgrass (*Zostera marina*) in Chesapeake Bay, USA. *Global Change Biology* 23: 3474-3483.

Loder, T.C., Reichard, R.P. 1981. The dynamics of conservative mixing in estuaries. *Estuaries* 4: 64-69.

Mallin, M.A., Burkholder, J.M., Cahoon, L.B., Posey, M.H. 2000. North and South Carolina Coasts. *Marine Pollution Bulletin* 41: 56-75.

Martin, J. L., McCutcheon, S.C. 1999. Hydrodynamics and transport for water quality modelling. Lewis Publishers, Washington, D.C., USA.

Moorman, M.C., S.A. Fitzgerald, L. N. Gurley, A. Rhoni-Aref, and K.A. Loftin. 2017. Water quality and bed sediment quality in the Albemarle Sound, North Carolina, 2012–14: U.S. Geological Survey Open-File Report 2016 –1171, 46 p., https://doi.org/10.3133/ofr20161171.

NCDEQ. 2021a. North Carolina Department of Environmental Quality. Pasquotank River Basin Water Resources Plan Draft. https://deq.nc.gov/about/divisions/water-resources/water-planning/basin-planning/water-resource-plans/pasquotank/draft

NCDEQ. 2021b. North Carolina Department of Environmental Quality. 2022 303d Listing and Delisting Methodology. May 2021, Raleigh, NC.

Paerl, H.W., Hall, N.S., Hounshell, A.G., Luettich, R.A. Jr., Osburn, C.L. 2019. Recent increase in catastrophic tropical cyclone flooding in coastal North Carolina, USA: Long-term observations suggest a regime shift. *Nature Scientific Reports* 9: Article number: 10620 (2019)

Paerl, H.W., Valdez, L.M., Joyner, A.R., Piehler, M.F., Lebo, M.E. 2004. Solving problems resulting from solutions: Evolution of a dual nutrient management strategy for the eutrophying Neuse River Estuary, North Carolina. *Environmental Science & Technology* 38: 3068-3073.

Peierls, B.L., Hall, N.S., Paerl, H.W. 2012. Non-monotonic responses of phytoplankton biomass accumulation to hydrologic variability: A comparison of two coastal plain North Carolina estuaries. *Estuaries and Coasts* 35:1376–1392.

Petus, C., Devlin, M., Teixera da Silva, E., Lewis, S., Waterhouse, J., Wenger, A., Bainbridge, Z., Tracey, D. 2018. Defining wet season water quality target concentrations for ecosystem conservation using empirical light attenuation models: A case study in the Great Barrier Reef (Australia). *Journal of Environmental Management* 213: 451-466.

Pinckney, J.L., Paerl, H.W., Harrington, M.B., Howe, K.E. 1998. Annual cycles of phytoplankton community-structure and bloom dynamics in the Neuse River Estuary North Carolina. *Marine Biology* 131: 371-381.

Prairie, Y.T. 1996. Evaluating the predictive power of regression models. *Canadian Journal of Fisheries and Aquatic Sciences* 53: 490-492.

Qi, S., Sun, G., Wang, Y., McNulty, S.G., Myers, J.A.M. 2009. Streamflow response to climate and landuse changes in a coastal watershed in North Carolina. *Transactions of the American Society of Agricultural and Biological Engineers* 52: 739-749.

RTI. 2013. Final Monitoring Report. Defense/Coastal/Estuarine Research Program (DCERP1). SERDP Project RC-1413.

Speight, H. 2020. Submerged aquatic vegetation in a low-visibility, low-salinity estuary in North Carolina: Identifying temporal and spatial distributions by sonar and local ecological knowledge. Ph.D. Dissertation. East Carolina University, Greenville, North Carolina. May 2020.

Spencer, R.G.M., Aiken, G.R., Dornblaser, M.M., Butler, K.D., Holmes, R.M., Fiske, G., Mann, P.J., Stubbins, A., 2013. Chromophoric dissolved organic matter export from U.S. Rivers. *Geophysical Research Letters* 40**:** 1575–1579. https://doi.org/10.1002/grl.50357.

Unsworth, R.F.K., Cullen, L.C., Pretty, J.N., Smith, D.J., Bell J.J. 2010. Economic and subsistence values of the standing stocks of seagrass fisheries: Potential benefits of no-fishing marine protected area management. *Ocean & Coastal Management* 53: 218-224.

Vahätalo, A. Wetzel, R.G., Paerl, H.W. 2005. Light absorption by phytoplankton and chromophoric dissolved organic matter in the drainage basin and estuary of the Neuse River, North Carolina (U.S.A.). *Freshwater Biology* 50: 477-493.

Van Dam, B.R., Wang, H. 2019. Decadal-scale acidification trends in adjacent North Carolina estuaries: Competing role of anthropogenic CO_2 and riverine alkalinity loads. Fronteirs in Marine Science doi: 10.3389/fmars.2019.00136

Wen, H. Perdrial, J., Abbott, B.W., Bernal, S., Dupass, R., Godsey, S.E., Harpold, A., Rizzo, D., Underwood, K., Adlerz, T., Sterle, G., Li, L. 2020. Temperature controls production but hydrology regulates export of dissolved organic carbon at the catchment scale. *Hydrology and Earth System Science* 24: 945-966. https://doi.org/10.5194/hess-24-945-2020.

Wilson, K.L., Lotze, H.K. 2019. Climate change projections reveal range shifts of eelgrass Zostera marina in the Northwest Atlantic. *Marine Ecology Progress Series* 620: 47-62.

Woodruff, D.L. Stumpf, R.P., Scope, J.A., Paerl, H.W. 1999. Remote estimation of water clarity in optically complex estuarine waters. *Remote Sensing of the Environment* 68:41-52.

Wright, W. 2016. Assessment of estuarine water quality at Cape Hatteras and Cape Lookout National Seashores, 2015 Data Summary. Natural Resource Data Series NPS/SECN/NRDS-2016/1056. National Park Service, Fort Collins, Colorado.

YSI. Technical Instructions. T627-01. Turbidity units and calibration solutions. YSI Turbidity Sensors. Xylem Inc. 2019.

Zimmerman, R.C. 2006. Light and photosynthesis in seagrass meadows. In: *Seagrasses: Biology, Ecology, and Conservation* (eds Larkum AWD, Orth RJ, Duarte CM), pp.303–321. Springer, Dordrecht,. The Netherlands.